MOLECULAR ONCOLOGY 9 (2015) 1510–1527

available at www.sciencedirect.com

ScienceDirect

www.elsevier.com/locate/molonc

Mechanism of irradiation-induced mammary cancer metastasis: A role for SAP-dependent Mkl1 signaling

Maria B. Asparuhova[a], *Chiara Secondini*[b], *Curzio Rüegg*[b], *Ruth Chiquet-Ehrismann*[a,c,*]

[a]*Friedrich Miescher Institute for Biomedical Research, Affiliated with the Novartis Institutes for Biomedical Research and the University of Basel, Maulbeerstrasse 66, 4058 Basel, Switzerland*
[b]*Department of Medicine, Faculty of Science, University of Fribourg, Rue Albert Gockel 1, 1700 Fribourg, Switzerland*
[c]*University of Basel, Faculty of Science, Basel, Switzerland*

ARTICLE INFO

Article history:
Received 18 December 2014
Received in revised form
19 March 2015
Accepted 11 April 2015
Available online 30 April 2015

Keywords:
Myocardin-related transcription factor-A (MRTF-A)
Extracellular matrix
Tumor rigidity
Cyclic mechanical strain
Gene regulation

ABSTRACT

Radiotherapy is a standard treatment after conservative breast cancer surgery. However, cancers relapsing within a previously irradiated area have an increased probability to metastasize. The mechanisms responsible for this aggressiveness remain unclear. Here, we used the clinically relevant 4T1 breast cancer model mimicking aggressive local relapse after radiotherapy to identify differences between tumors grown in untreated versus pre-irradiated mammary glands. Tumors grown within preirradiated beds were highly enriched in transcripts encoding collagens and other proteins building or modifying the extracellular matrix, such as laminin-332, tenascins, lysyl oxidases and matrix metalloproteinases. Type I collagen, known to directly contribute to tissue stiffening, and the pro-metastatic megakaryoblastic leukemia-1 (Mkl1) target gene tenascin-C were further investigated. Mammary tissue preirradiation induced Mkl1 nuclear translocation in the tumor cells *in vivo*, indicating activation of Mkl1 signaling. Transcript profiling of cultured 4T1 cells revealed that the majority of the Mkl1 target genes, including tenascin-C, required serum response factor (SRF) for their expression. However, application of dynamic strain or matrix stiffness to 4T1 cells converted the predominant SRF/Mkl1 action into SAP domain-dependent Mkl1 signaling independent of SRF, accompanied by a switch to SAP-dependent tumor cell migration. 4T1 tumors overexpressing intact Mkl1 became more metastatic within preirradiated beds, while tumors expressing Mkl1 lacking the SAP domain exhibited impaired growth and metastatic spread, and decreased Mkl1 target gene expression. Thus, we identified SAP-dependent Mkl1 signaling as a previously unrecognized mediator of aggressive progression of mammary tumors locally relapsing after radiotherapy, and provide a novel signaling pathway for therapeutic intervention.

* *Corresponding author*. Friedrich Miescher Institute for Biomedical Research, Maulbeerstrasse 66, CH-4058 Basel, Switzerland. Tel.: +41 61 697 24 94; fax: +41 61 697 39 76.
E-mail addresses: maria.asparuhova@fmi.ch (M.B. Asparuhova), chiara.secondini@unifr.ch (C. Secondini), curzio.ruegg@unifr.ch (C. Rüegg), Ruth.Chiquet@fmi.ch (R. Chiquet-Ehrismann).
http://dx.doi.org/10.1016/j.molonc.2015.04.003

1. Introduction

Breast cancer remains the second most common cancer worldwide with nearly 1.7 million new cases in 2012 (Ferlay et al., 2013). Radiotherapy, alone or in a combination with chemotherapy, is a widely used treatment after breast-saving surgery with proven therapeutic efficacy manifested by reduced incidence of locoregional and distant recurrences (Bartelink et al., 2001; Darby et al., 2011; Le Scodan et al., 2009). However, clinical evidence indicates that relapses occurring after radiotherapy are associated with increased metastatic potential and poor prognosis in breast (Mattsson et al., 1993; Vicini et al., 2003) as well as head and neck cancers (O'Brien et al., 1986; Vikram et al., 1984). This has also been confirmed experimentally, and tumors growing within a previously irradiated mammary tissue tend to be more invasive and to form more metastases (Barcellos-Hoff and Ravani, 2000; Bouchard et al., 2013; Lemay et al., 2011). Radiation-induced modifications of the tumor microenvironment are proposed to contribute to such aggressive behavior, a condition termed tumor bed effect (Barcellos-Hoff, 2010; Barcellos-Hoff et al., 2005; Milas et al., 1988), but the underlying molecular mechanisms remain elusive. The tumor microenvironment is known to be significantly different from healthy tissue, with a modified extracellular matrix (ECM) containing high levels of type I collagen, fibronectin, versican and tenascin-C (Adams et al., 2002; Brown et al., 1999; Kalluri and Zeisberg, 2006).

Breast cancer tissue is mechanically compromised and stiff, partly due to increased type I collagen deposition that has resulted in elastography as a commonly used diagnostic procedure (Levental et al., 2009; Paszek et al., 2005; Samani et al., 2003). Deposition of type I collagen linearly correlates with tissue stiffness in many different organs (Swift and Discher, 2014; Swift et al., 2013). Furthermore, increased mammographic density is associated with a significantly greater collagen amount and high susceptibility to breast cancer (Boyd et al., 2010; Li et al., 2005). Since radiation is known to induce fibrosis (O'Sullivan and Levin, 2003; Walker, 2001), tissue stiffening may be part of the reason for the pro-tumorigenic effect of radiotherapy. Increased rigidity of the tumor microenvironment results in mechanical forces that act on cancer cells and evoke compensatory responses mainly via RhoGTPase activation modulating actin dynamics (Butcher et al., 2009; Paszek et al., 2005).

Via its ability to induce actin polymerization, RhoA regulates the subcellular localization and activity of megakaryoblastic leukemia-1 (Mkl1) (Miralles et al., 2003; Vartiainen et al., 2007). Mkl1 is a member of the myocardin-related transcription factor (MRTF) family and a well-known transcriptional co-activator of serum response factor (SRF) (Cen et al., 2003; Miralles et al., 2003; Vartiainen et al., 2007; Wang et al., 2002). In unstimulated cells, Mkl1 is held inactive in the cytoplasm by reversible complex formation with G-actin (Miralles et al., 2003). Activation of RhoA feeds G-actin into the F-actin filaments, thus allowing nuclear import of G-actin-free Mkl1 and subsequent transcription of SRF target genes containing CArG boxes in their promoters (Miralles et al., 2003; Vartiainen et al., 2007). We have previously shown the presence of an atypical CArG box in the tenascin-C promoter and the involvement of SRF/Mkl1 signaling in its induction in fibroblasts (Asparuhova et al., 2011). Interestingly, induction of tenascin-C by cyclic mechanical strain did not require SRF, but instead depended on the potential DNA-binding SAP domain of Mkl1 (Asparuhova et al., 2011). Furthermore, we have recently described a gene set co-regulated with tenascin-C in a SAP-dependent/SRF-independent manner in non-transformed HC11 mammary epithelial cells (Gurbuz et al., 2014). The expression of this gene set was associated with high-proliferative poor-outcome classes in human breast cancer and a strongly reduced survival for patients independent of tumor grade. Tenascin-C is expressed by both cancer-associated fibroblasts as well as cancer epithelial cells, and is associated with tumorigenesis and cancer progression in different types of tumors (Brellier and Chiquet-Ehrismann, 2012). Strong evidence exists for its role in the primary tumor and the site of metastasis (Calvo et al., 2008; Minn et al., 2005; O'Connell et al., 2011; Oskarsson et al., 2011; Tavazoie et al., 2008). Tenascin-C has been identified among signature genes whose expression in primary breast tumors correlates with lung relapse (Minn et al., 2005). Also, high expression of tenascin-C in lung tissue of breast cancer patients correlates with shorter lung metastasis-free survival (Oskarsson et al., 2011). The important impact of tenascin-C on tumor cell survival, invasion, tumor angiogenesis and metastasis formation has also been recently demonstrated in a transgenic immune-competent mouse tumor model that mimics the high expression of tenascin-C observed in human cancer (Saupe et al., 2013).

In the current study, we investigated the effect of radiation on metastasis formation using the mouse 4T1 mammary carcinoma model. The 4T1 mammary carcinoma represents a clinically relevant animal model for human triple negative breast cancer (Dexter et al., 1978). The 4T1 metastatic disease develops spontaneously from the orthotopic site to multiple organs, thus encompassing all the stages of primary tumor growth, invasion, and metastasis including the tumor–host interactions in fully immunocompetent animals (Eckhardt et al., 2012; Pulaski and Ostrand-Rosenberg, 2001). This model has proven to be useful for mimicking aggressive local relapse of mammary tumors after radiotherapy (Kuonen et al., 2012; Monnier et al., 2008). Here, we provide novel insights into the mechanisms underlying the pro-metastatic effect of irradiation, and identify irradiation-induced SAP-dependent Mkl1 signaling as a previously unrecognized mediator of metastasis in mammary cancer.

2. Materials and methods

2.1. *Mouse model, irradiation, tumor growth and metastasis*

Primary tumors were initiated by orthotopic injection of 4T1 (ATCC; CRL-2539) mammary carcinoma cells into BALB/c mice (Charles River Laboratories) as described (Kuonen et al., 2012). Animal experiments were approved by the Swiss veterinary authorities. In some cases before

injection, the fourth mammary gland was locally irradiated with a single 20 Gy X-ray dose as described (Kuonen et al., 2012). Tumor volumes were assessed by caliper measurements. For lung metastasis quantification, mice were sacrificed 18–20 days after tumor cell injection. Lungs were dissected and fixed in 4% paraformaldehyde (PFA), embedded in paraffin, sectioned (4-μm thickness, 6 levels, 200-μm intervals), and stained with hematoxylin and eosin (H&E). Metastases per animal were counted using a Nikon Eclipse E600 and calculated as the total number of nodules/6 sections normalized to the final tumor volume.

2.2. Cell culture

Full length Mkl1 (FL-Mkl1) and the two Mkl1 mutants, mutB1-Mkl1 comprising mutations in the B1 domain and ΔSAP-Mkl1 lacking the SAP domain were previously described (Asparuhova et al., 2011). All Mkl1 variants were expressed as C-terminal red fluorescent protein (RFP)-tagged fusions. A control vector expressing RFP alone was described (Asparuhova et al., 2011).

4T1 mammary epithelial cells were grown in DMEM medium supplemented with 10% fetal calf serum (FCS, Invitrogen). In most of the experiments, cells were starved in 0.03% FCS/DMEM. To obtain 4T1 cells stably expressing FL-Mkl1-RFP (4T1-FL), mutB1-Mkl1-RFP (4T1-mutB1), ΔSAP-Mkl1-RFP (4T1-ΔSAP) or RFP alone (4T1 control), cells were transfected using FuGENE® 6 (Roche) and selected with Geneticin (Roche) for 14 days before RFP-based FACS sorting.

2.3. Cell proliferation, migration and invasion assays

Proliferation rates of the 4T1 cell lines were determined using a 5-bromo-2′-deoxyuridine (BrdU) incorporation assay (Roche) as described (Gurbuz et al., 2014).

Cell migration was assayed using transwell filters (Corning) as described (Gurbuz et al., 2014). After subjection to cyclic strain, 5×10^4 cells were plated in the upper chamber in serum-free DMEM. The lower chamber contained 10% FCS/DMEM. After migration for 22 h, cells were fixed and stained with crystal violet. Images of duplicate inserts were acquired on a Nikon Eclipse E600. Migration was quantified by measuring the area covered by migrated cells using ImageJ.

Cell invasion was assayed using the same procedure as for migration, except that: 1) the transwell filter was coated with 150 μl/cm^2 of growth factor-reduced Matrigel (BD Biosciences) diluted (1:3) with serum-free DMEM and allowed to solidify for 1 h at 37 °C; and 2) 2×10^5 cells after starvation for 24 h were seeded into the upper chamber.

2.4. Mechanical stimulation of cells

Equibiaxial cyclic strain (20%, 0.3 Hz) at 37 °C for 1 h was applied to starved 4T1 cells as described (Gurbuz et al., 2014). After strain, cells were either used in migration assays or lysed for RNA isolation.

For matrix stiffness experiments, 7×10^5 4T1 cells/well were seeded on fibronectin-coated polyacrylamide hydrogels of defined stiffness (0.5 or 4 kPa elastic modulus) in 35 mm dishes (Petrisoft™; Matrigen). Cells were cultured in 0.03% FCS/DMEM for 16 h before harvesting for RNA isolation.

2.5. RNA analyses by qRT-PCR

Total RNA from 4T1 cells or tissue homogenates was isolated using the RNeasy Mini Kit (Qiagen). Tissue samples (tumors and mammary glands) were collected, flash-frozen and homogenized in RLT buffer using a Dispomix Drive (Medic Tools). RNA was reverse transcribed and relative tenascin-C, Fos or carbonic anhydrase 12 (Car12) mRNA levels normalized to Gapdh were detected as described (Gurbuz et al., 2014). Relative collagen type I alpha 1 (Col1a1) or fibroblast growth factor-binding protein 1 (Fgfbp1) transcripts normalized to Gapdh, were measured using Platinum® SYBR® Green qPCR SuperMix-UDG with ROX (Invitrogen) and the following primers: Col1a1-F 5′-CCGGAAGAATACGTATCACCA-3′, Col1a1-R 5′-TCTGGGAAGCAAAGTTTCCT-3′; Fgfbp1-F 5′-ACTCACAGAAAGGTGTCCAC-3′, Fgfbp1-R 5′-TCCTGCTTCTCTGCTTATTCTG-3′. qPCR was performed as described (Gurbuz et al., 2014). Data from *in vivo* experiments were analyzed by the ΔCt method (Schmittgen and Livak, 2008), whereas data from *in vitro* experiments by the efficiency ΔΔCt method (Livak and Schmittgen, 2001) that included a further normalization to the 4T1 control.

2.6. Transcript profiling

Total RNA from tumor tissue samples as well as starved (for 48 h) 4T1 cell lines was extracted, converted into labeled cDNA and hybridized to Affymetrix GeneChip Mouse Gene 1.0 ST arrays. RMA-normalized expression values were calculated with the affy package from Bioconductor 2.4 (Gentleman et al., 2004), the genefilter package was used to remove probesets without Entrez gene annotation while only the probeset with the highest IQR was used for each Entrez gene. Differentially expressed genes were identified using moderated *t*-statistics calculated with the empirical Bayes method as implemented in the Bioconductor limma package (Smyth and Speed, 2003). To be considered as differentially expressed between tumors grown in nonirradiated and preirradiated mammary tissue, genes had to pass the filters: P-value $\leq$0.05, a log2 fold change $\geq$0.4 and a log2 average expression value $\geq$4.0. To be considered as differentially expressed between 4T1-FL and 4T1-mutB1 or 4T1-ΔSAP cells, genes had to meet the following criteria: a maximum P-value of 0.01 calculated with Benjamin–Hochberg false discovery correction, a minimum absolute linear fold change difference of 2.0 and a minimum log2 average expression value of 4.0. Microarray data files are available from the Gene Expression Omnibus (GEO; http://www.ncbi.nlm.nih.gov/geo/), accession numbers: GSE64193 (for tumor tissue samples) and GSE59459 (for cell lines).

2.7. Protein analyses by immunoblotting

Primary antibodies used: mAb65F13 anti-Mkl1 (Maier et al., 2008), MTn12 anti-tenascin-C (Aufderheide and Ekblom, 1988), anti-Fgfbp1 (bs-1768R, Bioss), anti-Car12 (15180-1-AP, Proteintech), anti-lamin A/C (612162, BD Biosciences)

and anti-Gapdh (ab9485, Abcam). After 24 h of starvation, whole-cell extracts from 4T1 lines were prepared in RIPA buffer as described (Maier et al., 2008). Secreted tenascin-C protein was detected in cell culture medium. For preparation of cytoplasmic, nuclear and ECM extracts, tumor samples were collected, flash-frozen and homogenized in lysis buffer containing 10 mM HEPES pH 7.9, 100 mM KCl, 1 mM EDTA, 1 mM DTT, 0.5% NP-40 and protease inhibitors, by using a Dispomix Drive. After centrifugation, the supernatant was collected as cytoplasmic extract. The nuclear pellets were washed with lysis buffer lacking NP-40, and extracted with 250 mM Tris–HCl pH 7.8, 100 mM KCl, 1 mM EDTA, 1 mM DTT, 0.5% NP-40, 20% glycerol shaking at 4 °C for 1 h, followed by centrifugation to clarify the nuclear extract. Proper fractionation was confirmed by Gapdh and lamin A/C presence as cytoplasmic and nuclear marker, respectively. The ECM fraction was obtained from the last pellet by extraction in RIPA buffer. Samples were run on SDS–PAGE and transferred to Immobilon-P membrane (Millipore). Ponceau S (0.1%) staining visualized bovine serum albumin (BSA) from the medium as a loading control. Proteins were detected using the antibodies listed above followed by HRP-conjugated secondary antibodies (MP Biomedicals) for detection with SuperSignal West Dura Chemiluminescent Substrate (ThermoFisher Scientific). Immunoblot signals were analyzed by densitometry using ImageQuant (Molecular Dynamics).

2.8. Immunohistochemistry and Masson's trichrome stain

Mouse tumors were dissected and fixed in 4% PFA, cryoprotected in 25% sucrose, embedded in OCT Tissue-Tek (Sakura), sectioned (12-μm thickness), and stained with H&E. Immunohistochemistry for tenascin-C, Fgfbp1, Car12 and Mkl1 was performed on the Ventana DiscoveryXT (Roche) by using the Research IHC Dap Map XT procedure. In brief, cryosections were subjected to antigen retrieval using standardCC1 (Roche) for detection with anti-Mkl1 (ARP37504_T100, Aviva Systems Biology), or protease buffer 3 (Roche) for Fgfbp1 and Car12. As secondary antibody, an HRP-conjugated polymer ImmPRESS (MP-7401, Vector Laboratories) was used preceded by R18-2 anti-rat IgGs (ab125900, Abcam) in the case of tenascin-C detection. All slides were counterstained with Hematoxylin II and Bluing Reagent (Roche).

Collagens were visualized using Accustain® Trichrome (Sigma–Aldrich) according to the manufacturer's procedure. Images were acquired on a Nikon Eclipse E600.

2.9. Statistical analysis

All grouped data are means ± SD. Statistical analysis was completed using GraphPad InStat v3.05. Differences between two groups were evaluated using a two-tailed Student's *t* test for parametric data or a Mann–Whitney *U* test for nonparametric data. Multiple comparisons were performed using one-way analysis of variance (ANOVA). Values of $P < 0.05$ were considered statistically significant.

3. Results

3.1. Stroma irradiation results in tumors with increased extracellular matrix deposition

To investigate the effect of mammary tissue irradiation on breast cancer progression, we pretreated the fourth mammary gland of BALB/c mice with a single dose of 20 Gy X-ray irradiation before implanting 4T1 tumor cells. This amount of irradiation corresponds to the cumulative dose of ~60 Gy delivered to breast cancer patients during fractionated therapy (Barton, 1995). Thus, the model of preirradiation recapitulates clinically relevant features of breast cancers locally relapsing after radiotherapy (Kuonen et al., 2012; Monnier et al., 2008). Mammary tissue preirradiation had no significant effect on 4T1 primary tumor volume (Figure 1A), while it strongly promoted lung metastasis formation (~4-fold increase) compared to mice with primary tumors growing in nonirradiated stroma (Figure 1B).

To explore the underlying molecular basis for the differential metastatic potential of tumors grown in preirradiated *vs.* nonirradiated mammary tissue, we performed transcript profiling of four tumor samples from each of the two mouse groups. A volcano plot filtering analysis (Figure 1C) using a minimal log2 fold change (logFC) of 0.4 and a maximal P value of 0.05 (presented in a −log10 P-scale) as the cutoff thresholds, identified 94 upregulated *vs.* 41 downregulated transcripts in tumors grown in preirradiated compared to tumors grown in nonirradiated beds (complete probeset lists and annotations are found in Supplementary Table S1). Interestingly, 47% of the transcripts whose expression in the primary tumors was significantly elevated by the mammary tissue preirradiation encode extracellular (EC) proteins as determined using the Ingenuity® software. The majority of these genes can be categorized to function in 1) building the extracellular matrix network and 2) matrix remodeling and regulation (Table 1). The first category consists of 7 genes encoding subunits of collagen type I, III, V, VI, XII and XIV in addition to members from the ECM structure-associated families of fibrillins (Fbn1), integrins (Itga2), laminins (Lama3, Lamb3, Lamc2), thrombospondins (Thbs2), tenascins (Tnc, Tnn) and lecticans (Vcan). In the second category, genes encoding extracellular proteases from the adamalysin (Adam12, Adamts5, 12) and matrix metalloproteinase (Mmp3, 10) families as well as their inhibitors (Serpina3n, Serpine1, Timp1) were found. Furthermore, the collagen crosslinking enzymes lysyl oxidases (Lox and Loxl1, 2) deserve special attention. Together with increased collagen deposition, the Lox-mediated collagen crosslinking is known to contribute to matrix stiffening and malignant progression in breast cancer (Barker et al., 2012; Cox et al., 2013; Erler et al., 2006; Levental et al., 2009; Paszek et al., 2005). Thus, the ECM-rich expression profile of tumors grown in preirradiated stroma led us to hypothesize that a major effect of irradiation is tumor stiffening.

To confirm this hypothesis, we monitored the expression of the major component of type I collagen, Col1a1, in the mammary gland and in 4T1 tumors developing in normal or preirradiated beds, since it has been demonstrated that the quantity of type I collagen present in tissues is directly

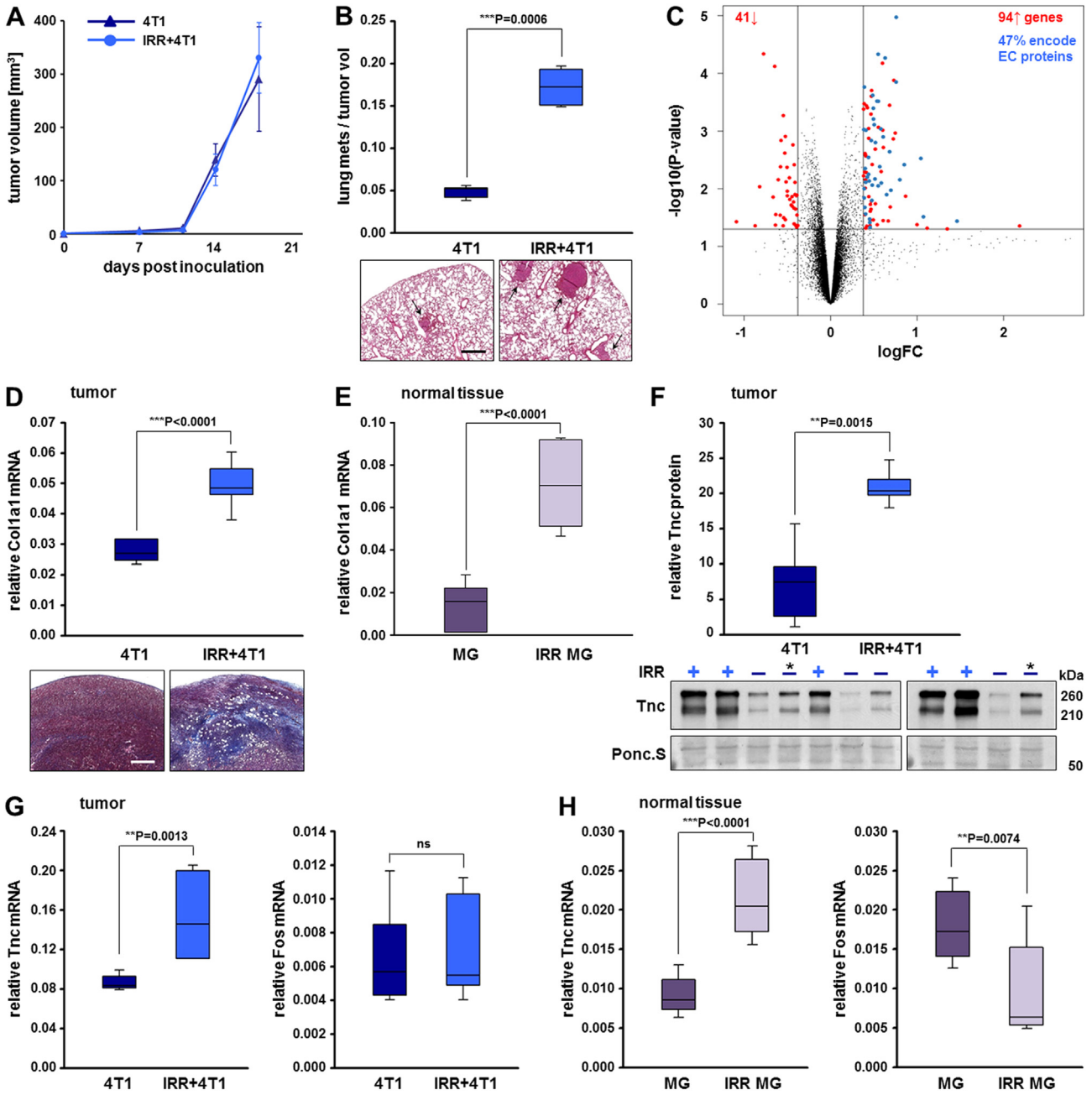

Figure 1 – Stroma irradiation results in tumors with increased extracellular matrix deposition. (A) Orthotopic tumor growth of 4T1 cells implanted in nonirradiated (4T1) or 20 Gy preirradiated mammary tissue (IRR+4T1). Tumor volumes were calculated from caliper measurements taken every 3–4 days. Data represent means ± SD for 7 mice per group. (B) Metastatic spread of the tumors described in (A). Number of spontaneous lung metastases in each animal was assessed 18 days after tumor initiation and normalized to the final tumor volume. A significant difference between the two groups, ***P < 0.001 is shown. Representative H&E-stained lung sections with tumor nodules marked by arrows are shown below the plot. Scale bar, 500 μm. (C) Volcano plot based on the log2 fold change (logFC; x-axis) and the P value in −log10 P-scale (y-axis) of all transcripts in the primary tumors described in (A). Transcripts that are similarly expressed between 4T1 and IRR+4T1 tumors are shown as black dots. The vertical lines represent 0.4 fold changes both upregulated (right side) and downregulated (left side), and the horizontal line represents a P value of 0.05. All colored dots in the plot represent the differentially expressed transcripts (94 upregulated and 41 downregulated) with statistical significance in IRR+4T1 *vs.* 4T1 tumors (complete probeset lists are found in Supplementary Table S1). The blue dots correspond to irradiation-induced genes encoding extracellular (EC) proteins as determined using the Ingenuity® software. (D) qRT-PCR analysis of Col1a1 transcripts normalized to Gapdh in the primary tumors described in (A). Data and statistical significance are expressed as in (A, B). Representative images of tumor sections stained for collagens (blue) by Masson's trichrome stain are shown below the plot. Scale bar, 500 μm. (E) qRT-PCR analysis of Col1a1 transcripts normalized to Gapdh in nonirradiated (MG) and irradiated (IRR MG) mammary glands in tumor-free mice. Means ± SD for 7 mice per group and significant differences between the two groups, ***P < 0.001 are shown. (F) Immunoblot analysis of

Table 1 – Functional categorization of ECM-associated genes significantly elevated in tumors grown in preirradiated compared to tumors grown in nonirradiated mammary tissue.

Gene symbol	Gene name	logFC	P-value
1. Building the matrix network			
1.1. Collagens[a,b]			
Col1a1	collagen, type I, alpha 1	0.5	4.02E-04
Col1a2	collagen, type I, alpha 2	0.5	3.03E-04
Col3a1	collagen, type III, alpha 1	0.6	1.26E-03
Col5a2	collagen, type V, alpha 2	0.6	4.65E-05
Col6a3	collagen, type VI, alpha 3	0.5	1.58E-03
Col12a1	collagen, type XII, alpha 1	0.4	2.86E-03
Col14a1	collagen, type XIV, alpha 1	0.4	9.66E-04
1.2. Genes encoding other structural proteins[c,d,e,f,g,h]			
Fbn1	fibrillin 1	0.8	1.07E-05
Itga2	integrin alpha 2	0.5	1.87E-02
Lama3	laminin, alpha 3	0.4	6.27E-03
Lamb3	laminin, beta 3	1.0	2.98E-03
Lamc2	laminin, gamma 2	0.7	1.06E-02
Thbs2	thrombospondin 2	0.5	6.19E-04
Tnc	tenascin C	0.6	5.41E-05
Tnn	tenascin N	0.4	7.72E-03
Vcan	versican	0.7	2.29E-03
2. Matrix remodeling and regulation			
2.1. Matrix cross-linking[i,j]			
Lox	lysyl oxidase	0.8	6.98E-03
Loxl1	lysyl oxidase-like 1	0.6	3.04E-04
Loxl2	lysyl oxidase-like 2	0.5	7.77E-04
2.2. Matrix degradation[k,l]			
Adam12	a disintegrin and metallopeptidase domain 12 (meltrin alpha)	0.5	1.98E-04
Adamts5	a disintegrin-like and metallopeptidase (reprolysin type) with thrombospondin type 1 motif, 5 (aggrecanase-2)	0.5	1.60E-02
Adamts12	a disintegrin-like and metallopeptidase (reprolysin type) with thrombospondin type 1 motif, 12	0.4	9.42E-04
Mmp3	matrix metallopeptidase 3	0.4	2.74E-02
Mmp10	matrix metallopeptidase 10	0.6	7.95E-03
Sulf1	sulfatase 1	0.5	3.80E-03
2.3. Inhibition of extracellular proteases[l,m]			
Serpina3n	serine (or cysteine) peptidase inhibitor, clade A, member 3N	1.5	3.65E-02
Serpine1 (PAI1)	serine (or cysteine) peptidase inhibitor, clade E, member 1	0.6	1.26E-02
Timp1	tissue inhibitor of metalloproteinase 1	0.4	5.63E-03

a, Ricard-Blum (2011); b, Hynes and Naba (2012); c, Ramirez and Sakai (2010); d, Schwartz (2010); e, Tsuruta et al. (2008); f, Calabro et al. (2014); g, Chiquet-Ehrismann and Tucker (2011); h, Ricciardelli et al. (2009); i, Barker et al. (2012); j, Cox et al. (2013); k, Bonnans et al. (2014); l, Roy and Walsh (2014); m, Heit et al. (2013).

proportional to tissue stiffness (Swift and Discher, 2014; Swift et al., 2013). Indeed, Col1a1 mRNA levels were 2-fold upregulated in tumors grown in preirradiated compared to tumors grown in nonirradiated beds (Figure 1D), and 4.6-fold upregulated in irradiated compared to normal mammary glands devoid of tumors (Figure 1E). Collagen deposition was confirmed by Masson's trichrome stain of tumor sections (Figure 1D).

Our attention was further attracted by tenascin-C, a prominent mechanoresponsive gene (Chiquet-Ehrismann and Chiquet, 2003), whose irradiation-induced expression in tumors developing in preirradiated beds might contribute to the observed tumor aggressiveness. Therefore, we investigated the expression levels of tenascin-C in tumors growing in nonirradiated or preirradiated beds by immunoblotting (Figure 1F). Tenascin-C protein expression in tumor extracts

tenascin-C protein expression in ECM fractions of the primary tumors described in (A); (−) and (+) indicate 4T1 and IRR+4T1 tumors, respectively; (*) indicates a sample loaded for comparison on both gels. The box plot represents a densitometric quantification of the immunoblot signals. Tenascin-C protein expression is normalized to the loading control visualized by Ponceau S staining of the membranes. Means ± SD for 5 mice per group and a significant difference between the two groups, $^{**}P < 0.01$, are shown. (G) qRT-PCR analysis of tenascin-C and Fos mRNA levels normalized to Gapdh mRNA in the primary tumors described in (A). Data represent means ± SD for 7 mice per group. Significant differences between the two groups, $^{**}P < 0.01$, ns = not significant. (H) qRT-PCR analysis of tenascin-C and Fos mRNA levels normalized to Gapdh mRNA in the tumor-free mammary gland tissues described in (E). Data and statistical significance are expressed as in (E).

was 3-fold upregulated by stromal preirradiation. In addition, qRT-PCR analysis showed a robust increase in tenascin-C mRNAs in the 4T1 tumors developing in the preirradiated *vs.* nonirradiated bed, while Fos mRNA expression remained unchanged (Figure 1G). Furthermore, irradiation of the mammary tissue in tumor-free mice also exhibited increased tenascin-C but not Fos mRNA levels compared to nonirradiated mammary glands (Figure 1H), confirming the essential role that irradiation plays in the induction of tenascin-C.

3.2. *Irradiation induces Mkl1 nuclear translocation*

Since tenascin-C is part of a gene set that is tightly regulated by Mkl1 and associated with poor prognosis in breast cancer patients (Gurbuz et al., 2014), we decided to investigate whether Mkl1 signaling functions in the 4T1 tumor model *in vivo* and whether it contributes to the increased aggressiveness of stiff tumors developing in preirradiated mammary tissue.

Mkl1 transcript levels did not significantly differ between tumors grown in a preirradiated *vs.* nonirradiated stroma. However, a measure for transcriptional activity of the ubiquitously expressed Mkl1 (Wang et al., 2002) is its nuclear translocation induced by mitogenic or mechanical stimulation (Maier et al., 2008; Miralles et al., 2003; Zhao et al., 2007). To test whether irradiation and tumor stiffening induce Mkl1 transcriptional activity, we examined the subcellular distribution of Mkl1 by immunoblot analysis using cytoplasmic and nuclear extracts of 4T1-derived tumors grown in normal or preirradiated stroma (Figure 2A and B). Separation of the nuclear from the cytoplasmic components was verified by the presence of lamin A/C and Gapdh as a nuclear and cytoplasmic marker, respectively. Mkl1 was detected in both compartments of the tumor tissues with a predominant nuclear localization approximating 76% of the total cellular Mkl1 protein in tumors grown in preirradiated stroma, as opposed to an elevated cytoplasmic localization (~90%) in tumors grown in nonirradiated beds.

Consistent with the immunoblot and qRT-PCR data (Figure 1F and G), immunohistochemical analysis of 4T1-derived tumors revealed an increased tenascin-C protein expression in tumors developing in a preirradiated mammary tissue compared to a moderate expression in control tumors (Figure 2C). Strong tenascin-C expression was also detected in the preirradiated adjacent tumor stroma, indicating that both host stromal and injected tumor epithelial cells are the source of tenascin-C in the 4T1 tumor model. Despite the ubiquitous Mkl1 immunostaining in tumors developing in both nonirradiated and preirradiated stroma, there was a clear correlation between the elevated tenascin-C expression and nuclear localization of Mkl1 in tumors grown in preirradiated beds (Figure 2C and D).

These results suggested a stimulating effect of irradiation on Mkl1 transcriptional activity in the tumor context *in vivo*.

3.3. *Mkl1 induces primary tumor growth and lung metastasis formation*

To analyze the requirement of different Mkl1 functional domains for Mkl1-mediated signaling in the 4T1 tumor model, we generated 4T1 cell lines stably expressing either the C-terminal RFP-tagged full length Mkl1 (4T1-FL), Mkl1-RFP lacking the SAP domain (4T1-ΔSAP) or Mkl1-RFP with a mutated SRF-interaction site located in the B1 domain (4T1-mutB1) (Figure 3A). None of the Mkl1 variants had cytotoxic effects and no changes in viability or cell morphology were observed. The three cell lines were FACS sorted to express similar Mkl1-RFP protein levels. Expression was verified by immunoblotting and appeared to be significantly elevated compared to the endogenous Mkl1 protein in 4T1 control cells stably transfected with an RFP-encoding vector (Figure 3B). 4T1-FL cells were shown to express 7-fold higher levels of Mkl1 transcripts compared to 4T1 control cells (Asparuhova et al., 2011).

First, we assessed the proliferative and invasive ability of the 4T1 cell lines using BrdU incorporation and Matrigel invasion assays, respectively. Compared to 4T1 control cells, FL- or ΔSAP-Mkl1 overexpressing 4T1 cells showed a significant increase in BrdU uptake into newly synthesized DNA until they reached confluence 72 h later (Figure 3C). In contrast, 4T1-mutB1 cells expressing an Mkl1 with impaired binding to SRF behaved like 4T1 control cells. The invasion analysis revealed that 4T1 cells expressing FL- or ΔSAP-Mkl1 were 3–6-fold more invasive than 4T1 control ($P < 0.001$) or 4T1-mutB1 cells ($P < 0.001$; Figure 3D). Thus, we concluded that overexpression of Mkl1 induced proliferation and invasion in an SRF-dependent/SAP-independent manner.

Next, we orthotopically implanted each of the 4T1 stable lines into BALB/c mice and monitored tumor growth for 20 days. The results demonstrated that FL-, ΔSAP- but not mutB1-Mkl1 overexpression significantly accelerated primary tumor growth (Figure 3E) in agreement with the proliferation behavior of the 4T1 lines in culture (cf. Figure 3C). Thus, overexpression of Mkl1 appeared to be more potent in the induction of primary tumor growth than the mammary tissue irradiation evoking nuclear translocation of endogenous Mkl1 protein (cf. Figure 1A). Together with the enhanced tumor growth, increased numbers of metastatic nodules in the lungs were observed with the least effect seen in mutB1-Mkl1 tumors (Figure 3F), suggesting a prominent role for SRF/Mkl1 signaling in promoting primary tumor growth and spontaneous lung metastasis formation.

3.4. *SRF-dependent tenascin-C, Fgfbp1 and Car12 expression in 4T1 cells*

With the aim to identify Mkl1 target genes in 4T1 cells, we used microarray analysis to compare the transcriptomes of 4T1 stable lines expressing Mkl1 variants. The threshold for SRF- or SAP-dependence was taken as a 2-fold reduction in gene expression levels in 4T1-mutB1 or 4T1-ΔSAP compared to 4T1-FL cells. Three groups of interest were established as presented in the Venn diagram in Figure 4A. The largest cohort contained 246 genes that depended on the function of the B1 site but not the SAP domain for their induction (SRF-dependent/SAP-independent), while each of the two SAP-dependent groups consisted of less than 40 genes. In contrast, in our previous study using the non-transformed HC11 mammary epithelial cells many more transcripts required the SAP domain of Mkl1 for their expression (Gurbuz et al., 2014). Among them were tenascin-C as well as fibroblast growth factor-binding protein 1 (Fgfbp1) and

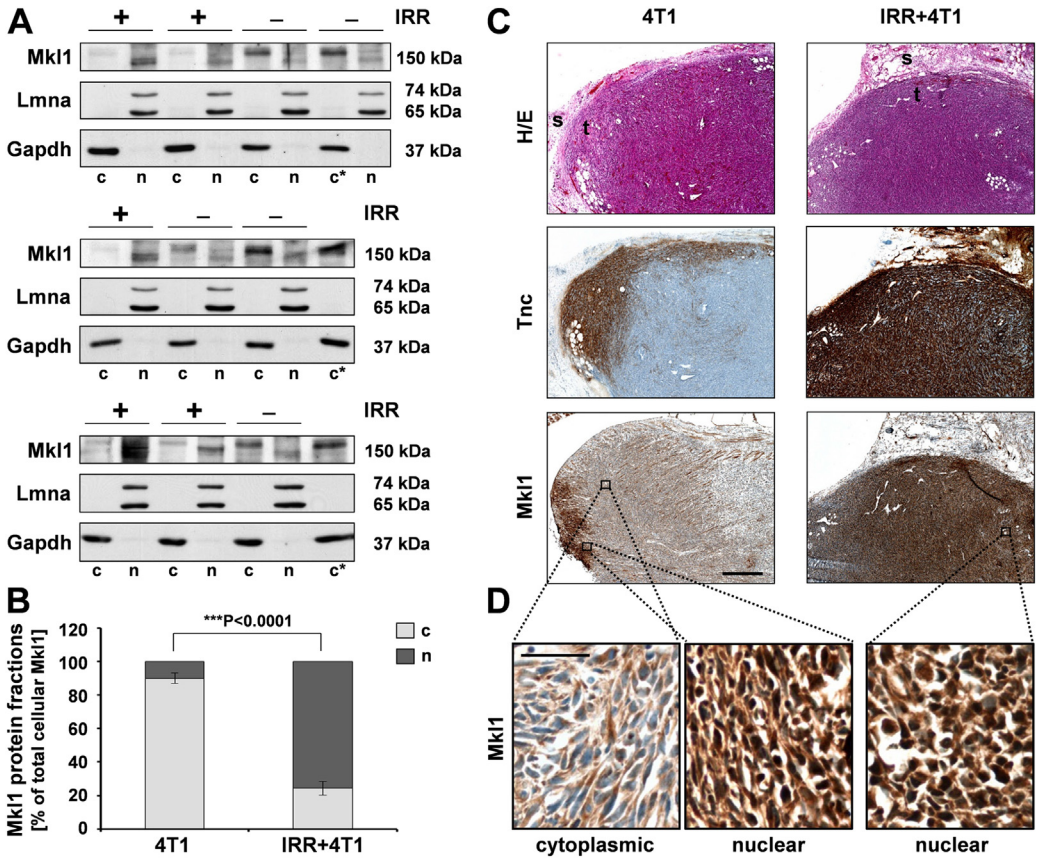

Figure 2 – Irradiation induces Mkl1 nuclear translocation. (A) Immunoblot analysis of Mkl1 protein expression in cytoplasmic (c) and nuclear (n) extracts of 4T1-derived tumors grown in nonirradiated (–) or 20 Gy preirradiated (+) mammary tissue. Successful fractionation and equal loading were verified by the detection of lamin A/C (Lmna) and Gapdh as a nuclear and cytoplasmic protein, respectively. (*) indicates a sample reloaded for comparison on each gel. The Mkl1 proteins detected in the two fractions migrated at slightly different molecular weights, most likely due to phosphorylation shown to promote Mkl1 cytoplasmic localization (Muehlich et al., 2008). Relevant bands and molecular weight markers (in kDa) are indicated on the left and right of each panel, respectively. (B) Densitometric analysis of the immunoblots shown in (A). The Mkl1 protein in the cytoplasmic and nuclear fractions of the tumor samples is normalized to the respective loading control and expressed as percent of the total cellular Mkl1 protein (taken as 100%). Means ± SD for 5 mice per group and a significant difference between the two groups, ***$P < 0.001$, are shown. (C) Example of an H&E stain (H/E) and immunohistochemical detection of tenascin-C (Tnc) and Mkl1 in sequential sections of the tumor types described in (A). Scale bar, 500 μm; t = tumor, s = adjacent tumor stroma. (D) Higher magnification images of the boxed area in the bottom panels of (C) stained with anti-Mkl1. Scale bar, 50 μm.

carbonic anhydrase 12 (Car12), genes encoding extracellular tumorigenic proteins (Abuharbeid et al., 2006; Chiche et al., 2009; Czubayko et al., 1997; Ivanov et al., 2001), which were now present in the group of SRF-dependent/SAP-independent genes (Figure 4B). Transcripts of these genes were about 3-fold downregulated in mutB1- compared to FL-Mkl1 expressing 4T1 cells (Figure 4B).

To confirm that the three transcripts are indeed differentially expressed in the different 4T1 lines, qRT-PCR analysis was performed. In comparison with cells expressing the control vector or mutB1-Mkl1, a significant increase in tenascin-C, Fgfbp1 and Car12 mRNA levels was detected in cells expressing FL- or ΔSAP-Mkl1 (Figure 4C). Finally, the SRF-dependent/SAP-independent expression of tenascin-C, Fgfbp1 and Car12 was confirmed on the protein level, showing greatly reduced expression of each of the three proteins in mutB1-Mkl1 cells compared to FL- or ΔSAP-Mkl1 cells (Figure 4D).

3.5. *Matrix stiffness and cyclic mechanical strain trigger SAP-dependent Mkl1 signaling in 4T1 cells*

To investigate the function of Mkl1 signaling in 4T1 cells in mechanically compromised environments, we reproduced tissue stiffening *in vitro*. 4T1 cells were cultured on fibronectin-coated polyacrylamide hydrogels of defined stiffnesses, corresponding to either 0.5 or 4 kPa elastic modulus. This corresponds to the average stiffnesses measured in healthy (compliant) and diseased (rigid) mammary tissues, respectively (Butcher et al., 2009; Lopez et al., 2011; Paszek et al., 2005). Tenascin-C, Fgfbp1, Car12 and Fos gene expression was investigated in these cells by qRT-PCR analyses (Figure 5A). The stiffness sensed by 4T1 control and 4T1-FL cell lines grown on 4-kPa matrices caused a moderate upregulation of tenascin-C, Fgfbp1 and Car12 mRNA levels compared to the respective lines on 0.5-kPa matrices (black and gray

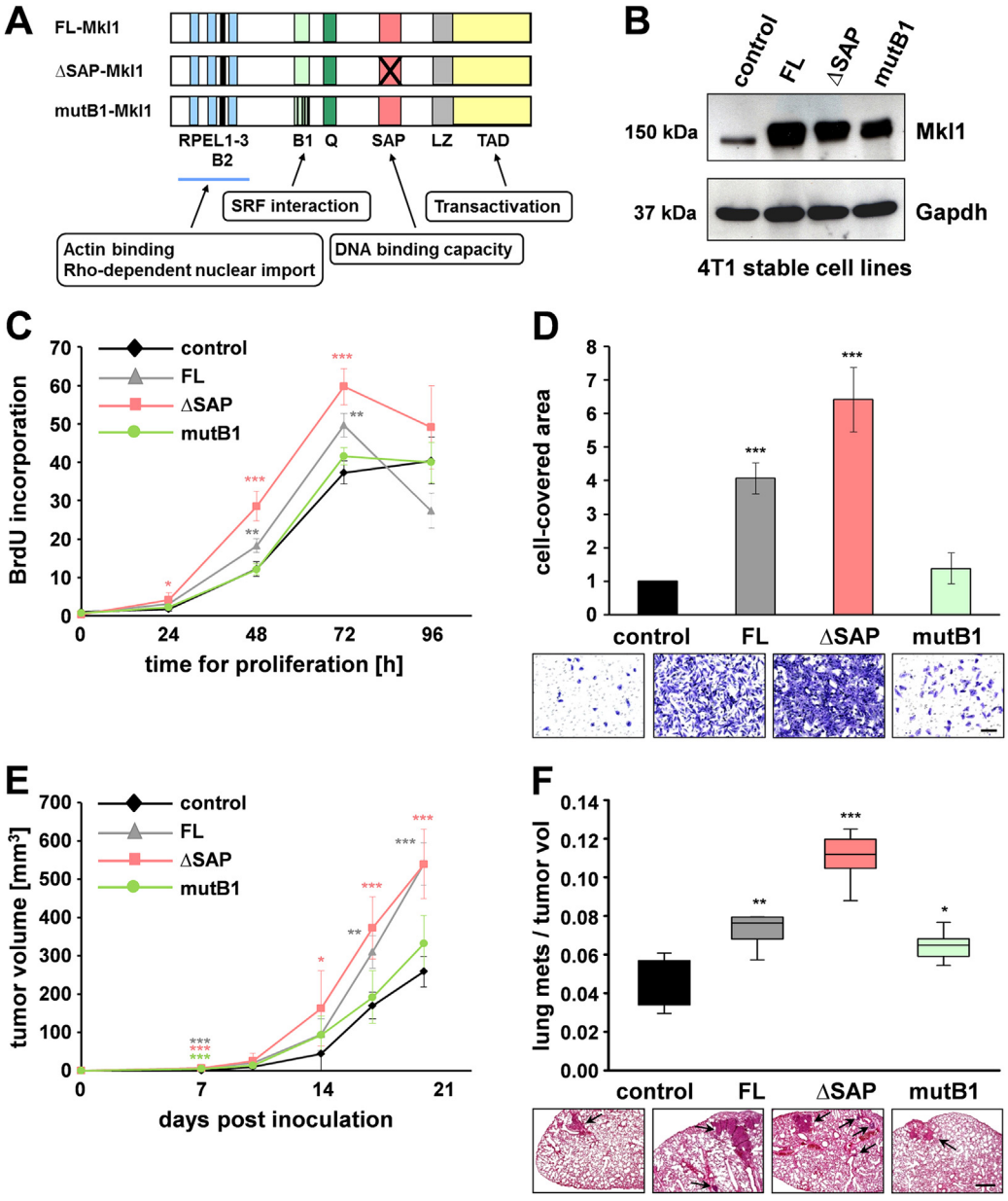

Figure 3 – Mkl1 induces primary tumor growth and lung metastasis formation. (A) Schematic representation of mouse Mkl1 constructs used for the generation of stable 4T1 cell lines. A full length Mkl1 (FL-Mkl1) construct comprises all functional domains present in the endogenous protein: RPEL1-3, actin binding motifs; B1 and B2, basic domains; Q, glutamine-rich domain; SAP, homology domain with a DNA binding capacity found in SAF-A/B, Acinus, PIAS; LZ, leucine zipper-like domain; TAD, transactivation domain. ΔSAP-Mkl1 is a variant lacking the SAP domain, and mutB1-Mkl1 is a full-length protein with a mutated SRF-binding site. All Mkl1 variants contain an RFP-tag at the C-terminus. (B) Immunoblot with mAb65F13 of Mkl1 proteins in whole-cell extracts from 4T1 lines stably transfected with either a control vector encoding RFP alone or with vectors encoding FL-, ΔSAP-, or mutB1-Mkl1 proteins. Anti-Gapdh served as loading control. (C) SRF-dependent/SAP-independent proliferation of 4T1 cells *in vitro*. Proliferation rates of the 4T1 cell lines described in (B) were assessed by BrdU incorporation into newly synthesized DNA immediately after plating (0 h) as well as at 24, 48, 72 and 96 h. Means ± SD from four independent experiments and significant differences to the 4T1 control line at the time point 0, ***$P < 0.001$, **$P < 0.01$, *$P < 0.05$ are shown. (D) SRF-dependent/SAP-independent invasion of 4T1 cells *in vitro*. Cell invasion through Matrigel-coated filters was assessed and quantified by measuring the area on the underside of the filters covered with cells that have degraded the Matrigel and traversed the filter. Means ± SD from three independent experiments and significant differences to the 4T1 control line, ***$P < 0.001$ are shown. Representative images of fixed and stained cells of each of the cell lines are shown below the graph. Scale bar, 200 μm. (E) Orthotopic tumor growth of the 4T1 cell lines in mice. Tumor volumes were calculated from caliper measurements taken every 3–4 days. Data represent means ± SD for 5 mice per group. Significant differences to the 4T1 control group, ***$P < 0.001$, **$P < 0.01$, *$P < 0.05$. (F) Metastatic potential of the 4T1 lines presented by a box-and-whisker plot. Number of spontaneous lung metastases in each animal was assessed 20 days after tumor initiation and normalized to the final tumor volume. Data and statistical significance are expressed as in (E). Representative images of H&E-stained lung sections in each of the experimental groups are shown below the plot. Arrows point to metastatic nodules. Scale bar, 500 μm.

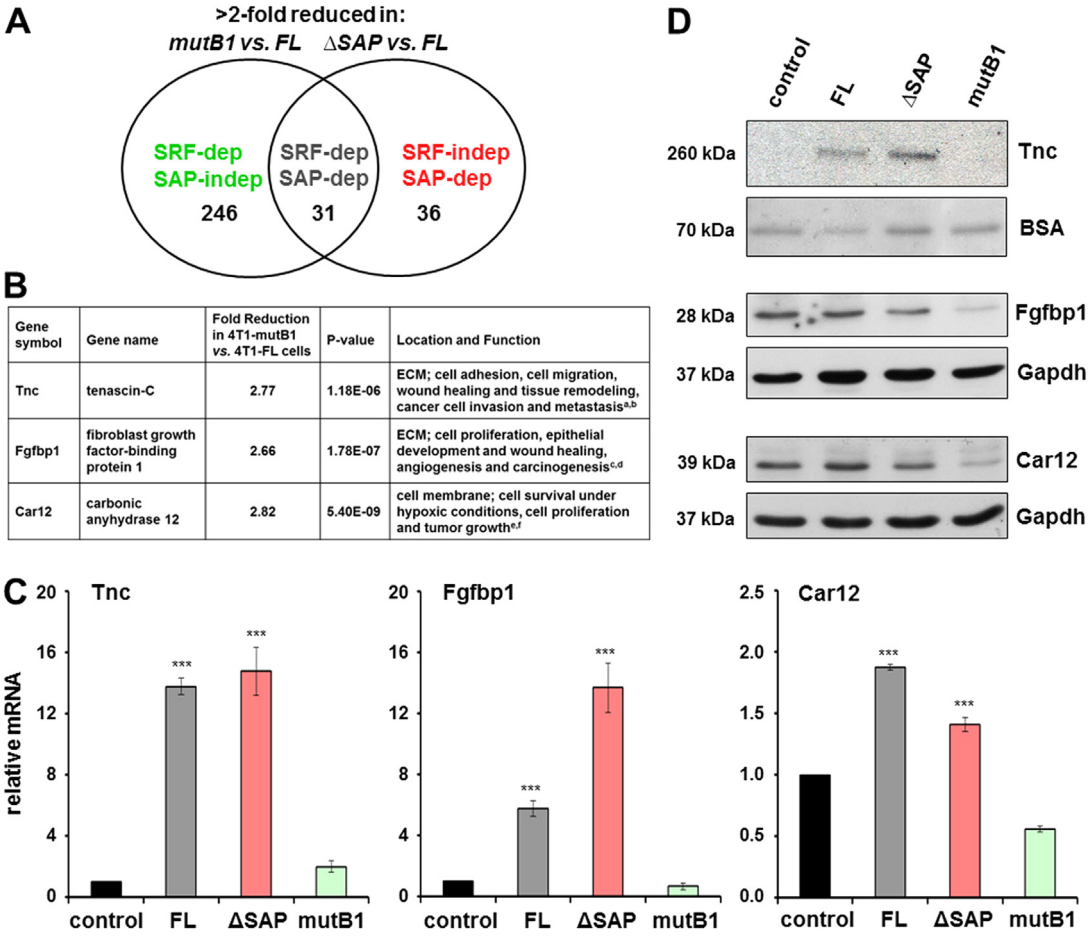

Figure 4 – SRF-dependent tenascin-C, Fgfbp1 and Car12 expression in 4T1 cells. (A) Venn diagram representing a summary of transcript profiling data classifying Mkl1 target genes into three groups: SRF-dependent/SAP-independent, SRF-dependent/SAP-dependent and SRF-independent/SAP-dependent. The number of transcripts, which are more than 2-fold reduced in either 4T1-mutB1 or 4T1-ΔSAP cells when compared to 4T1-FL cells are shown. (B) Summary listing profiling data, location and functions for the three SRF-dependent/SAP-independent genes, tenascin-C, Fgfbp1 and Car12. Fold reduction and P-value for each of the transcripts in 4T1-mutB1 compared to 4T1-FL cells are shown. References: [a]Brellier and Chiquet-Ehrismann, 2012; [b]Chiquet-Ehrismann and Chiquet, 2003; [c]Czubayko et al., 1997; [d]Abuharbeid et al., 2006; [e]Ivanov et al., 2001; [f]Chiche et al., 2009. (C) qRT-PCR analysis of tenascin-C, Fgfbp1 and Car12 mRNA levels in the stable 4T1 cell lines. Values normalized to Gapdh are expressed relative to the values of 4T1 control cells. Means ± SD from four independent experiments and significant differences to the 4T1 control line, ***P < 0.001 are shown. (D) Immunoblot analysis for tenascin-C, Fgfbp1 and Car12 proteins in the 4T1 cell lines. Secreted tenascin-C protein was detected in cell culture media and BSA from the medium visualized by Ponceau S staining served as loading control. Fgfbp1 and Car12 proteins were detected in whole-cell extracts. Anti-Gapdh served as loading control. Relevant bands and molecular weight markers (in kDa) are indicated on the right and left of each panel, respectively.

bars). However, the substrate rigidity was differently sensed by the 4T1-ΔSAP and 4T1-mutB1 cell lines (red and green bars). While the induction of tenascin-C, Fgfbp1 and Car12 transcripts in cells cultured on 0.5-kPa matrices was SRF-dependent/SAP-independent, the rigidity experienced by cells cultured on 4 kPa-stiff matrices induced a switch to SRF-independent/SAP-dependent Mkl1 signaling. This was demonstrated by a significant downregulation of the mRNA levels in 4T1-ΔSAP (red bars) and an upregulation in 4T1-mutB1 (green bars) cells grown on 4-kPa matrices. In contrast, the mechanoresponsive SRF target gene Fos (Cen et al., 2003), used as a control, showed an SRF-dependent/SAP-independent expression in either condition tested (last panel).

It has recently been demonstrated that inhibition of cell spreading due to a lack of matrix stiffness can be overcome by externally applied cyclic strain, suggesting that similar mechanotransduction mechanisms sense stiffness and stretch (Throm Quinlan et al., 2011). Therefore, we tested the influence of cyclic mechanical strain on Mkl1-mediated signaling in 4T1 cells (Figure 5B). Gene expression in cells at rest exhibited the standard SRF-dependent/SAP-independent pattern (Figure 5B, rest). Furthermore, in 4T1 control and 4T1-FL cell lines, cyclic strain caused a slight increase in tenascin-C, Fgfbp1 and Car12 mRNA levels compared to the respective lines at rest (Figure 5B, black and gray bars). Similarly to the effect of stiffness, cyclic strain switched the SRF-

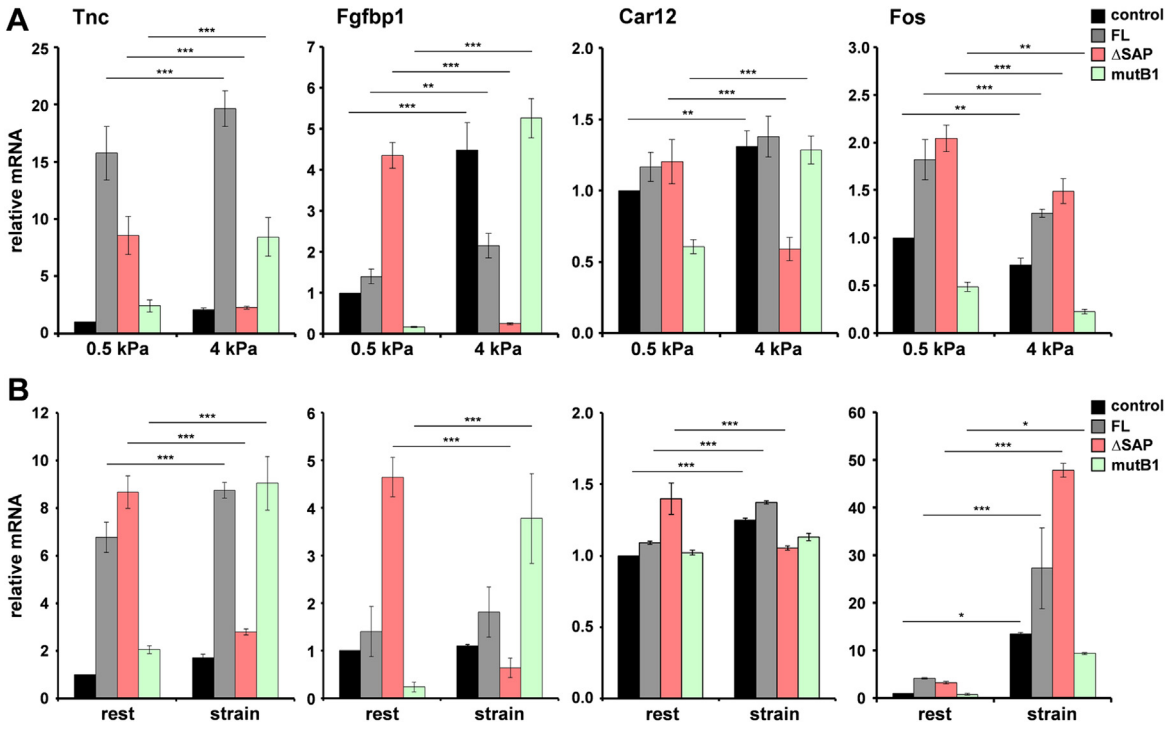

Figure 5 – Matrix stiffness (A) and cyclic mechanical strain (B) trigger SAP-dependent tenascin-C, Fgfbp1 and Car12 gene expression. (A) qRT-PCR analysis of tenascin-C, Fgfbp1, Car12 and Fos mRNA levels in the stable 4T1 cell lines cultured on fibronectin-coated polyacrylamide hydrogels with a stiffness corresponding to either 0.5 (compliant) or 4 (stiff) kPa elastic modulus. Values normalized to Gapdh are expressed relative to the values of 4T1 control cells grown on 0.5 kPa matrices. Data represent means ± SD from three independent experiments. Significant differences to the corresponding cell line on 0.5 kPa matrices, ***P < 0.001, **P < 0.01. (B) Gene expression analyzed as in (A) in the stable 4T1 cell lines without mechanical stimulation (rest) or subjected to cyclic strain (20%; 0.3 Hz) for 1 h. Data are expressed relative to the resting 4T1 control line, and represented as in (A). Significant differences to the corresponding cell line at rest, ***P < 0.001, *P < 0.05.

dependent/SAP-independent tenascin-C, Fgfbp1 and Car12 expression to SRF-independent/SAP-dependent (red and green bars). Thus, the mRNA levels were significantly downregulated in the stretched 4T1-ΔSAP (red bars) and upregulated in the stretched 4T1-mutB1 cells (green bars). This was not observed for the unrelated Fos gene that remained an SRF/Mkl1 target in resting as well as in strained cells (last panel). Furthermore, cyclic strain caused a super-induction of Fos mRNA by 7–15-fold in all 4T1 lines compared to the respective unstimulated ones, pointing to additional Mkl1-independent pathways for Fos activation by strain.

Taken together, these results demonstrate that substrate stiffness and tensile stress potentiate SAP-dependent Mkl1 signaling in 4T1 tumor cells.

3.6. *Cyclic mechanical strain induces SAP-dependent 4T1 cell migration*

To test whether the SAP-dependent Mkl1 target gene expression induced by cyclic strain has any consequences on cell behavior *in vitro*, we analyzed the influence of cyclic strain on 4T1 cell migration using transfilter migration assays (Figure 6). Similarly to the effect on cell invasion (cf. Figure 3D), FL- or ΔSAP-Mkl1 significantly induced cell motility by 4- and 4.5-fold, respectively, compared to 4T1 control cells, whereas mutB1-Mkl1 had no effect (Figure 6, rest). Cyclic strain application to the 4T1 stable lines before plating them in Boyden chambers significantly induced the migration of 4T1 control as well as 4T1-FL and 4T1-mutB1 cells compared to the migration of the respective unstimulated lines (Figure 6). This induction was strongly dependent on the Mkl1 SAP domain, which was manifested by ~4-fold inhibition of the migration of stretched compared to unstimulated 4T1-ΔSAP cells (Figure 6).

These results suggest that SAP-dependent Mkl1 signaling triggered by mechanical forces acting on tumor cells induces cell migration.

3.7. *Irradiation induces SAP-dependent tumor progression*

Since mechanical stimulation of 4T1 cells converts Mkl1 target gene expression from SRF- into SAP-dependent and positively influences cell migration, we examined whether the pro-metastatic effect of irradiation *in vivo* could be due to induction of SAP-dependent Mkl1 signaling. To address this question, we grafted 4T1-ΔSAP or 4T1-FL cells in normal or preirradiated mammary tissue. Compared to the growth in normal stroma, 4T1-FL-derived tumors developing in preirradiated beds had smaller volumes for about 10–12 days

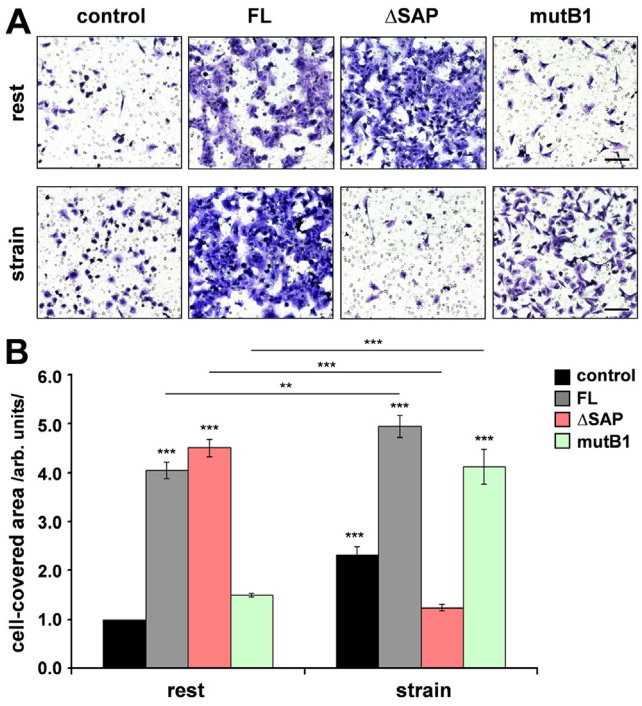

Figure 6 – Cyclic mechanical strain induces SAP-dependent 4T1 cell migration. (A) The stable 4T1 cell lines without mechanical stimulation (rest) or subjected to cyclic strain (20%; 0.3 Hz) for 1 h were harvested and plated for Transwell migration assays using filters with 8 μm pore size. Representative images of fixed and stained cells of each of the cell lines that have migrated to the underside of the filter are shown. Scale bar, 200 μm. (B) Quantification of cell migration was performed by measuring the area on the lower side of the filter covered with cells. Experimental values are expressed relative to the values of 4T1 control cells not exposed to strain. Means ± SD from three independent experiments and significant differences to the 4T1 control line at rest, ***P < 0.001, **P < 0.01 are shown.

(Figure 7A). Towards day 18, this difference in the tumor volume became insignificant. In contrast, 4T1-ΔSAP-derived tumors developing in a preirradiated stroma showed a significant retardation in their growth for the entire time period tested compared to their growth in nonirradiated beds. A major difference in the effect of irradiation on the metastatic potential of the two tumor types was observed. While 4T1-FL-derived tumors grown in a preirradiated bed were highly metastatic, almost no metastases could be detected in the lungs of mice bearing 4T1-ΔSAP-derived tumors grown in preirradiated beds (Figure 7B). Thus, preirradiation of the microenvironment strongly impaired the metastatic spread of 4T1-ΔSAP cells compared to their metastatic ability when grown in a nonirradiated stroma (Figure 7B). Furthermore, stroma preirradiation presumably increased the stiffness of both 4T1-FL- and 4T1-ΔSAP-derived tumors since their Col1a1 transcripts were significantly upregulated compared to the respective tumors grown in normal beds (Figure 7C). This was confirmed by Masson's trichrome collagen stain of tumor sections (Figure 7D and Supplementary Figure S1). Consistent with the increased collagen accumulation, which can be considered as a sign for irradiation-induced tumor stiffening, immunohistochemical and immunoblot analysis revealed an elevated nuclear localization of Mkl1 protein in both 4T1-FL- and 4T1-ΔSAP-derived tumors developing in preirradiated beds in comparison with the prominent Mkl1 cytoplasmic localization in tumors grown in nonirradiated mammary tissue (Supplementary Figure S2).

Finally, qRT-PCR analysis revealed a significant reduction in tenascin-C mRNA by 2.1-fold in 4T1-ΔSAP-derived tumors grown in a preirradiated *vs.* nonirradiated stroma (Figure 7E). In addition, a strong downregulation by 3.8-fold of Fgfbp1 and a weak but significant decrease of Car12 mRNA levels were measured in 4T1-ΔSAP tumors developing in the preirradiated *vs.* nonirradiated bed (Figure 7F). In contrast, irradiation increased tenascin-C, Fgfbp1 and Car12 expression in 4T1-FL-derived tumors (Figure 7E and F). Conversely, Fos mRNA levels were significantly decreased by the irradiation in 4T1-FL but not in 4T1-ΔSAP tumors (Figure 7F). The SAP-dependent tenascin-C, Fgfbp1 and Car12 expression induced by the preirradiation was also confirmed at protein level (Supplementary Figure S3).

The model in Figure 8 combines our *in vitro* and *in vivo* findings. It indicates that increased matrix stiffness and dynamic strain trigger SAP-dependent expression of the Mkl1 target genes tenascin-C, Fgfbp1 and Car12 in cultured 4T1 cells. Induction of the same genes is also found in tumors grown in preirradiated stroma exhibiting an ECM- and collagen-enriched expression profile, which may result in stiffer tumors. As a consequence, tumors developing within the preirradiated microenvironment exhibit increased metastatic progression. The right part of the model suggests that decreasing the tumor matrix rigidity through application of ECM-targeting agents will impede the metastatic disease by inhibition of the SAP-dependent Mkl1 signaling.

4. Discussion

Local breast cancer relapses within a previously irradiated field in patients who underwent conservative breast cancer surgery and radiotherapy are associated with an increased risk of developing metastasis and poor prognosis compared to recurrences outside of the irradiated area (Mattsson et al., 1993; Vicini et al., 2003). To date, there are no effective options to prevent or treat metastatic dissemination in these relapses. Using a well-characterized model of murine breast cancer, we identified irradiation-induced SAP-dependent Mkl1 signaling as an essential mediator fostering metastatic growth of tumors developing in preirradiated mammary tissue (Figure 8).

Comparison of tumors grown in preirradiated *vs.* nonirradiated mammary glands revealed an interesting change of gene expression. Tumors grown within preirradiated mammary tissue expressed increased levels of ECM encoding genes, including collagens I, III, V, VI, XII and XIV as well as ECM modifying enzymes, such as lysyl oxidases and metalloproteinases, and their inhibitors. Interestingly, both chains forming the major collagen type I were upregulated together with other collagen types found to be crucial for type I collagen assembly and deposition. These are collagen type III (Liu et al., 1997), type V (Sun et al., 2011), type XII (Chiquet et al., 2014)

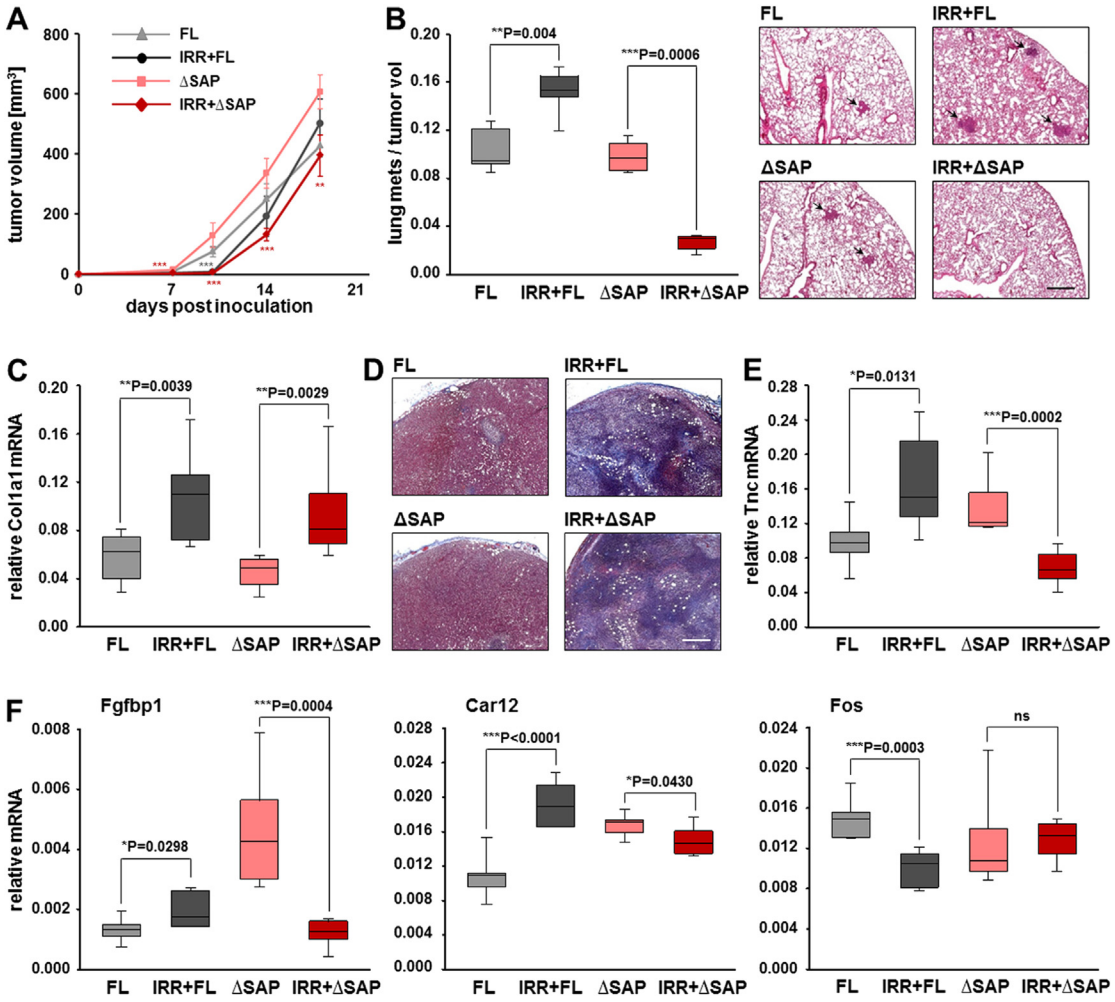

Figure 7 – Irradiation induces SAP-dependent tumor progression. (A) Orthotopic tumor growth of 4T1-FL and 4T1-ΔSAP cells implanted in either nonirradiated or 20 Gy preirradiated stroma, designated as FL, IRR + FL, ΔSAP and IRR + ΔSAP tumors. Tumor volumes were calculated from caliper measurements taken every 3–4 days. Data are means ± SD for 7 mice per group. For statistical analyses, each of the two tumor types, FL and ΔSAP grown in nonirradiated mammary tissue, was compared to the respective tumor type grown in preirradiated stroma. Significant differences, ***P < 0.001, **P < 0.01, *P < 0.05. (B) Metastatic spread of the tumors described in (A). Number of spontaneous lung metastases in each animal was assessed 18 days after tumor initiation and normalized to the final tumor volume. Statistical significance is expressed as in (A). Right panels show representative H&E-stained lung sections with metastatic nodules pointed by arrows. Scale bar, 500 μm. (C) qRT-PCR analysis of Col1a1 transcript normalized to Gapdh in the primary tumors described in (A). Data and statistical significance are expressed as in (A). (D) Representative images of tumor sections stained for collagens (blue) by Masson's trichrome stain. Scale bar, 500 μm. Additional images are shown in Supplementary Figure S1. (E, F) qRT-PCR analysis of tenascin-C (E), Fgfbp1, Car12 and Fos (F) mRNA levels normalized to Gapdh mRNA in the primary tumors described in (A). Data and statistical significance are expressed as in (A); ns = not significant.

and type XIV (Ansorge et al., 2009). Furthermore, collagen type VI is known to affect the tumor microenvironment, thus promoting tumor progression (Chen et al., 2013). Together with the increased collagen deposition, three lysyl oxidase genes were also induced by the stroma preirradiation. This is expected to further contribute to matrix stiffening and malignant progression in breast cancer (Barker et al., 2012; Cox et al., 2013; Erler et al., 2006; Levental et al., 2009; Paszek et al., 2005). Implication in cancer progression has already been demonstrated for most of the remaining irradiation-induced ECM proteins. This is particularly evident for tenascin-C and tenascin-W which is encoded by the Tnn gene (Brellier et al., 2012), laminin-332 (Guess and Quaranta, 2009), as well as the matrix metalloproteinases and their inhibitors (Roy and Walsh, 2014).

Ingenuity® pathway analysis of the entire list of genes induced in tumors grown in preirradiated mammary glands revealed TGF-β1 signaling as the main pathway affected (data not shown). This is reminiscent of a related study, where mice were subjected to whole body irradiation before implantation of Trp53-deficient orthotopic mammary transplants (Nguyen et al., 2011). The authors observed an accelerated tumor development in the irradiated mice and transcript profiling revealed TGF-β1 in the central node of the network induced in tumors from irradiated animals. Clearly, an induction of TGF-β1 signaling in stiff tumors is to be expected and

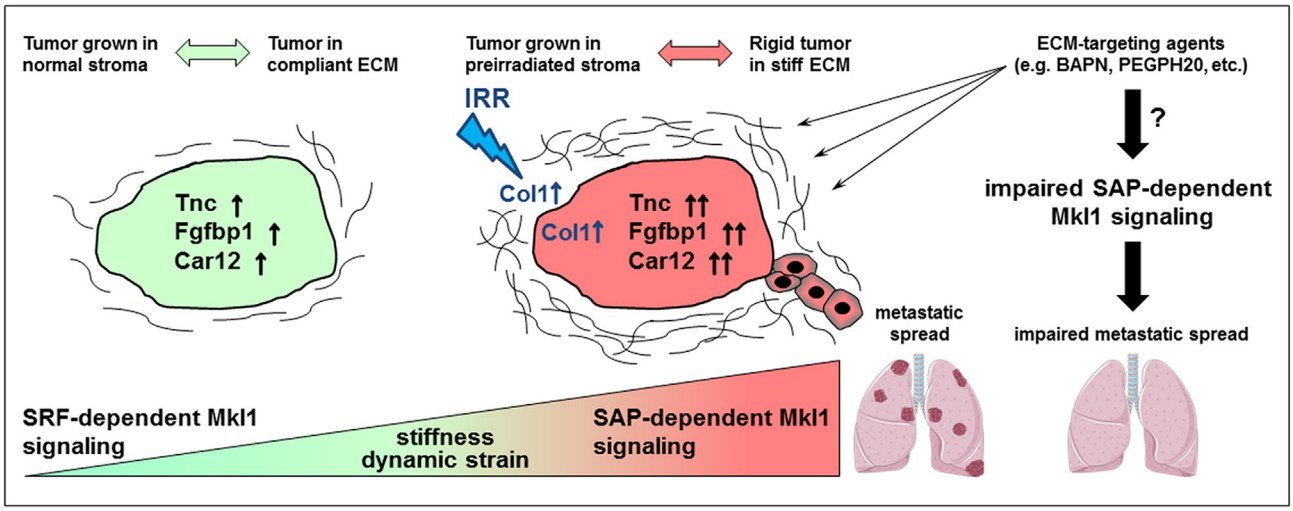

Figure 8 – Model for the role of SAP-dependent Mkl1 signaling in irradiation (IRR)-induced mammary cancer metastasis. The model summarizes the results from our *in vitro* and *in vivo* experiments using the 4T1 breast tumor model. Increased matrix stiffness and dynamic strain trigger SAP-dependent expression of the Mkl1 target genes tenascin-C, Fgfbp1 and Car12 in cultured 4T1 cells. SAP-dependent Mkl1 signaling resulting in the induction of the same genes is also triggered in 4T1 tumors developing within a preirradiated stroma. The increased ECM and in particular collagen deposition in these tumors suggests that they are stiffer and with higher stromal content than tumors grown within nonirradiated mammary tissue. Thereby, we hypothesize that irradiation-induced tissue stiffening mediates SAP-dependent Mkl1 signaling and aggressive progression of mammary tumors locally relapsing after radiotherapy. Our study identifies tenascin-C, Fgfbp1 and Car12 as irradiation-induced Mkl1 target genes with a potential functional implication in the metastatic process. The right part of the model suggests that application of ECM-targeting agents able to decrease the tumor matrix rigidity, such as BAPN (β-aminopropionitrile) or the hyaluronidase PEGPH20, will impede cancer progression by inhibition of the SAP-dependent Mkl1 signaling.

may represent a vicious cycle due to stretch-induced TGF-β1 activation fostering mesenchymal to epithelial transition (O'Connor and Gomez, 2014). Furthermore, we have recently demonstrated that TGF-β induces a novel Mkl1 variant in human adipose-derived mesenchymal stem cells (Scharenberg et al., 2014).

Our *in vivo* data are supported by *in vitro* experiments demonstrating that mechanical stimulation of 4T1 mammary carcinoma cells by dynamic strain or matrix stiffness, converted the predominant SRF/Mkl1 into SAP-dependent Mkl1 signaling. Furthermore, strain application induced tumor cell migration in a SAP-dependent manner, which prompted us to further investigate SAP domain-dependent Mkl1 function in cancer progression. The first published study associating Mkl1 with cancer showed that depletion of Mkl1/2 proteins reduced motility, invasion and colonization of metastatic tumor cells (Medjkane et al., 2009). Since then, several studies using different experimental models reported divergent results for the role of SRF/Mkl1 signaling in tumorigenesis and cancer progression (Descot et al., 2009; Leitner et al., 2010; Yoshio et al., 2010). Work from our laboratory provides clear evidence for the SAP domain-dependent action of Mkl1 as a tumor-promoting pathway in two distinct mammary epithelial cell types, HC11 (Gurbuz et al., 2014) and 4T1 (this paper). It remains to be seen whether Mkl1 induces target gene expression through SAP acting as a putative DNA binding domain, or indirectly through a yet unknown interaction partner and alternative signaling events. Proteins other than SRF were shown to bind and regulate the activity of Mkl1 for specific functions. For example, Mkl1 was implicated in TGFβ-induced epithelial-to-mesenchymal transition via an interaction with Smad3 transcription factor (Morita et al., 2007). Furthermore, a factor called suppressor of cancer cell invasion (SCAI) has been identified as an Mkl1-interacting partner that reduced β1-integrin expression through inhibition of the Mkl1/SRF transcriptional complex (Brandt et al., 2009). We are currently investigating the downstream events triggered by mechanical stimulation that determine the switch in the Mkl1 mode of action between SRF transactivation *vs.* its SAP-dependent transcriptional activity. Force-induced post-translational modifications of Mkl1 or its interactions with the epigenetic machinery are possible scenarios. The distinct expression pattern of Mkl1 protein with a strongly elevated nuclear localization in tumors grown in preirradiated beds and an elevated cytoplasmic localization of more slowly migrating Mkl1 in tumors grown in normal stroma, support the notion that post-translational modifications, such as phosphorylation shown to induce transcriptional changes (Muehlich et al., 2008), might determine the switch. Recent studies have also reported Mkl1 to induce chromatin reorganizations enabling transcription of distinct genes in a cell- and context-specific manner (Flouriot et al., 2014; Hanna et al., 2009; Yang et al., 2013; Zhang et al., 2007). The potential involvement of epigenetic modifications in mechanical strain-induced Mkl1 target gene expression could explain the changes we have seen in the migration behavior triggered by cyclic strain in cells overexpressing Mkl1.

The focus of the current study on tenascin-C, Fgfbp1 and Car12 was determined by the fact that the three genes were common targets of Mkl1 in HC11 (Gurbuz et al., 2014) and 4T1 cells, and were previously characterized as part of a SAP-dependent gene set associated with high-proliferative poor-outcome classes in human breast cancer and a strongly reduced survival rate for patients independent of tumor grade (Gurbuz et al., 2014). Fgfbp1 and Car12 were found overexpressed in different tumor types (Abuharbeid et al., 2006; Ivanov et al., 2001), and were associated with tumor growth and either angiogenesis (Fgfbp1) (Czubayko et al., 1997) or hypoxia (Car12) (Chiche et al., 2009). However, to date their role in metastatic dissemination is not extensively investigated. In contrast, the contribution of tenascin-C to breast cancer progression is well recognized (Calvo et al., 2008; Minn et al., 2005; O'Connell et al., 2011; Oskarsson et al., 2011; Tavazoie et al., 2008). Tenascin-C, as an ECM protein secreted by both fibroblasts and epithelial cells in response to irradiation and subsequent activation of SAP-dependent Mkl1 signaling, might itself affect the rigidity of the tumor tissue and influence tumor cell survival and motility by a positive tumorigenic feedback loop. Furthermore, a tenascin-C-rich matrix might provide a source for storage and presentation of growth factors to stimulate tumor growth, since many growth factors were found to bind to tenascin-C (De Laporte et al., 2013). A similar autocrine stimulation of tumor cells can be envisaged for Fgfbp1 and Car12. Once released in the extracellular space, they can exhibit specific physiological functions in favor of tumor growth, e.g., by enhancing FGF signaling (Aigner et al., 2001) or enabling cell survival under hypoxic conditions (Chiche et al., 2009). From a therapeutic and/or prognostic point of view, the future discovery of other genes co-regulated with tenascin-C, Fgfbp1 and Car12 and responsive to: 1) mechanical stimulation; and 2) SAP-dependent Mkl1 signaling, might result in a metastasis gene signature characteristic of stiff tumors with high stromal content and high interstitial tissue pressure.

The availability or new discovery of pharmacologic inhibitors targeting the stiff tumor microenvironment, and thereby reducing SAP-dependent Mkl1 signaling to inhibit mammary cancer progression, will open novel opportunities for translational and clinical studies. Since the 4T1-derived tumors grown in preirradiated stroma exhibit increased collagen accumulation, it will be interesting to test whether inhibition of collagen crosslinking using cell-soluble β-aminopropionitrile (BAPN) (Erler et al., 2006; Pickup et al., 2013) or a LOX-specific antibody (Cox et al., 2013; Erler et al., 2006), would prevent fibrosis and impede cancer progression by reducing SAP-dependent Mkl1 signaling (Figure 8). In this respect, also the enzymatic degradation of stromal hyaluronan using PEGPH20 could be considered, since in addition to hyaluronan it also reduces the expression of Col1a1, Col5a1 and tenascin-C in prostate cancer xenografts (Jiang et al., 2012; Provenzano et al., 2012).

In summary, our findings support a link between tumor matrix stiffening and cancer progression, and place SAP domain-dependent Mkl1 signaling as a central pathway mechanistically linking the two processes. This mechanism is an important mediator of irradiation-enhanced metastatic growth. Our data raise the possibility that inhibition of SAP-dependent Mkl1 signaling by application of existing or novel pharmacological substances, decreasing extracellular matrix rigidity after irradiation, could be a useful therapeutic approach against breast cancer relapse and progression.

Competing interests

The authors declare that they have no competing interests.

Authors' contributions

MBA and RCE conceived the study. MBA designed and performed all *in vitro* experiments. CR consulted and approved the *in vivo* experiments. CS planned and performed irradiation and orthotopic injections of tumor cells in host mice, followed tumor growth and dissected mouse organs. Further processing of mouse tissues and downstream experiments were designed and performed by MBA. MBA analyzed and interpreted the data and wrote the paper, assisted by RCE, CR and CS. RCE supervised the study.

Acknowledgments

We thank Hubertus Kohler for FACS service, Stephane Thiry and Tim Roloff for the microarray processing and data analysis, Augustyn Bogucki and Sandrine Bichet for carrying out immunohistochemistry, and Matthias Chiquet and Richard P. Tucker for critical reading of the manuscript. This work was supported by grants from the Cancer League of Basel, the Swiss Cancer League and the Swiss National Science Foundation 3100A0-120235 and 31003A_135584 to R.C.E., and the Swiss Cancer League, the Swiss National Science Foundation 3100A0_135738 and the Medic Foundation to C.R.

Appendix A. Supplementary data

Supplementary data related to this article can be found at http://dx.doi.org/10.1016/j.molonc.2015.04.003.

REFERENCES

Abuharbeid, S., Czubayko, F., Aigner, A., 2006. The fibroblast growth factor-binding protein FGF-BP. Int. J. Biochem. Cell Biol. 38, 1463–1468.

Adams, M., Jones, J.L., Walker, R.A., Pringle, J.H., Bell, S.C., 2002. Changes in tenascin-C isoform expression in invasive and preinvasive breast disease. Cancer Res. 62, 3289–3297.

Aigner, A., Butscheid, M., Kunkel, P., Krause, E., Lamszus, K., Wellstein, A., Czubayko, F., 2001. An FGF-binding protein (FGF-BP) exerts its biological function by parallel paracrine stimulation of tumor cell and endothelial cell proliferation through FGF-2 release. Int. J. Cancer 92, 510–517.

Ansorge, H.L., Meng, X., Zhang, G., Veit, G., Sun, M., Klement, J.F., Beason, D.P., Soslowsky, L.J., Koch, M., Birk, D.E., 2009. Type XIV collagen regulates fibrillogenesis: premature collagen

fibril growth and tissue dysfunction in null mice. J. Biol. Chem. 284, 8427–8438.
Asparuhova, M.B., Ferralli, J., Chiquet, M., Chiquet-Ehrismann, R., 2011. The transcriptional regulator megakaryoblastic leukemia-1 mediates serum response factor-independent activation of tenascin-C transcription by mechanical stress. FASEB J. 25, 3477–3488.
Aufderheide, E., Ekblom, P., 1988. Tenascin during gut development: appearance in the mesenchyme, shift in molecular forms, and dependence on epithelial-mesenchymal interactions. J. Cell Biol. 107, 2341–2349.
Barcellos-Hoff, M., 2010. Stromal mediation of radiation carcinogenesis. J. Mammary Gland Biol. Neoplasia 15, 381–387.
Barcellos-Hoff, M.H., Park, C., Wright, E.G., 2005. Radiation and the microenvironment – tumorigenesis and therapy. Nat. Rev. Cancer 5, 867–875.
Barcellos-Hoff, M.H., Ravani, S.A., 2000. Irradiated mammary gland stroma promotes the expression of tumorigenic potential by unirradiated epithelial cells. Cancer Res. 60, 1254–1260.
Barker, H.E., Cox, T.R., Erler, J.T., 2012. The rationale for targeting the LOX family in cancer. Nat. Rev. Cancer 12, 540–552.
Bartelink, H., Horiot, J.C., Poortmans, P., Struikmans, H., Van den Bogaert, W., Barillot, I., Fourquet, A., Borger, J., Jager, J., Hoogenraad, W., Collette, L., Pierart, M., 2001. Recurrence rates after treatment of breast cancer with standard radiotherapy with or without additional radiation. N. Engl. J. Med. 345, 1378–1387.
Barton, M., 1995. Tables of equivalent dose in 2 Gy fractions: a simple application of the linear quadratic formula. Int. J. Radiat. Oncol. Biol. Phys. 31, 371–378.
Bonnans, C., Chou, J., Werb, Z., 2014. Remodelling the extracellular matrix in development and disease. Nat. Rev. Mol. Cell Biol. 15, 786–801.
Bouchard, G., Bouvette, G., Therriault, H., Bujold, R., Saucier, C., Paquette, B., 2013. Pre-irradiation of mouse mammary gland stimulates cancer cell migration and development of lung metastases. Br. J. Cancer 109, 1829–1838.
Boyd, N.F., Martin, L.J., Bronskill, M., Yaffe, M.J., Duric, N., Minkin, S., 2010. Breast tissue composition and susceptibility to breast cancer. J. Natl. Cancer Inst. 102, 1224–1237.
Brandt, D.T., Baarlink, C., Kitzing, T.M., Kremmer, E., Ivaska, J., Nollau, P., Grosse, R., 2009. SCAI acts as a suppressor of cancer cell invasion through the transcriptional control of beta1-integrin. Nat. Cell Biol. 11, 557–568.
Brellier, F., Chiquet-Ehrismann, R., 2012. How do tenascins influence the birth and life of a malignant cell? J. Cell. Mol. Med 16, 32–40.
Brellier, F., Martina, E., Degen, M., Heuze-Vourc'h, N., Petit, A., Kryza, T., Courty, Y., Terracciano, L., Ruiz, C., Chiquet-Ehrismann, R., 2012. Tenascin-W is a better cancer biomarker than tenascin-C for most human solid tumors. BMC Clin. Pathol. 12, 14.
Brown, L.F., Guidi, A.J., Schnitt, S.J., Van De Water, L., Iruela-Arispe, M.L., Yeo, T.K., Tognazzi, K., Dvorak, H.F., 1999. Vascular stroma formation in carcinoma in situ, invasive carcinoma, and metastatic carcinoma of the breast. Clin. Cancer Res. 5, 1041–1056.
Butcher, D.T., Alliston, T., Weaver, V.M., 2009. A tense situation: forcing tumour progression. Nat. Rev. Cancer 9, 108–122.
Calabro, N.E., Kristofik, N.J., Kyriakides, T.R., 2014. Thrombospondin-2 and extracellular matrix assembly. Biochim. Biophys. Acta 1840, 2396–2402.
Calvo, A., Catena, R., Noble, M.S., Carbott, D., Gil-Bazo, I., Gonzalez-Moreno, O., Huh, J.I., Sharp, R., Qiu, T.H., Anver, M.R., Merlino, G., Dickson, R.B., Johnson, M.D., Green, J.E., 2008. Identification of VEGF-regulated genes associated with increased lung metastatic potential: functional involvement of tenascin-C in tumor growth and lung metastasis. Oncogene 27, 5373–5384.
Cen, B., Selvaraj, A., Burgess, R.C., Hitzler, J.K., Ma, Z., Morris, S.W., Prywes, R., 2003. Megakaryoblastic leukemia 1, a potent transcriptional coactivator for serum response factor (SRF), is required for serum induction of SRF target genes. Mol. Cell. Biol. 23, 6597–6608.
Chen, P., Cescon, M., Bonaldo, P., 2013. Collagen VI in cancer and its biological mechanisms. Trends Mol. Med. 19, 410–417.
Chiche, J., Ilc, K., Laferrière, J., Trottier, E., Dayan, F., Mazure, N.M., Brahimi-Horn, M.C., Pouysségur, J., 2009. Hypoxia-inducible carbonic anhydrase IX and XII promote tumor cell growth by counteracting acidosis through the regulation of the intracellular pH. Cancer Res. 69, 358–368.
Chiquet-Ehrismann, R., Chiquet, M., 2003. Tenascins: regulation and putative functions during pathological stress. J. Pathol. 200, 488–499.
Chiquet, M., Birk, D.E., Bönnemann, C.G., Koch, M., 2014. Collagen XII: protecting bone and muscle integrity by organizing collagen fibrils. Int. J. Biochem. Cell Biol. 53, 51–54.
Chiquet-Ehrismann, R., Tucker, R.P., 2011. Tenascins and the importance of adhesion modulation. Cold Spring Harb. Perspect. Biol. 3, a004960.
Cox, T.R., Bird, D., Baker, A.M., Barker, H.E., Ho, M.W., Lang, G., Erler, J.T., 2013. LOX-mediated collagen crosslinking is responsible for fibrosis-enhanced metastasis. Cancer Res. 73, 1721–1732.
Czubayko, F., Liaudet-Coopman, E., Aigner, A., Tuveson, A., Berchem, G., Wellstein, A., 1997. A secreted FGF-binding protein can serve as the angiogenic switch in human cancer. Nat. Med. 3, 1137–1140.
Darby, S., McGale, P., Correa, C., Taylor, C., Arriagada, R., Clarke, M., Cutter, D., Davies, C., Ewertz, M., Godwin, J., Gray, R., Pierce, L., Whelan, T., Wang, Y., Peto, R., 2011. Effect of radiotherapy after breast-conserving surgery on 10-year recurrence and 15-year breast cancer death: meta-analysis of individual patient data for 10,801 women in 17 randomised trials. Lancet 378, 1707–1716.
De Laporte, L., Rice, J.J., Tortelli, F., Hubbell, J.A., 2013. Tenascin C promiscuously binds growth factors via its fifth fibronectin type III-like domain. PLoS One 8, e62076.
Descot, A., Hoffmann, R., Shaposhnikov, D., Reschke, M., Ullrich, A., Posern, G., 2009. Negative regulation of the EGFR-MAPK cascade by actin-MAL-mediated Mig6/Errfi-1 induction. Mol. Cell 35, 291–304.
Dexter, D.L., Kowalski, H.M., Blazar, B.A., Fligiel, Z., Vogel, R., Heppner, G.H., 1978. Heterogeneity of tumor cells from a single mouse mammary tumor. Cancer Res. 38, 3174–3181.
Eckhardt, B.L., Francis, P.A., Parker, B.S., Anderson, R.L., 2012. Strategies for the discovery and development of therapies for metastatic breast cancer. Nat. Rev. Drug Discov. 11, 479–497.
Erler, J.T., Bennewith, K.L., Nicolau, M., Dornhofer, N., Kong, C., Le, Q.T., Chi, J.T.A., Jeffrey, S.S., Giaccia, A.J., 2006. Lysyl oxidase is essential for hypoxia-induced metastasis. Nature 440, 1222–1226.
Ferlay, J., Soerjomataram, I., Ervik, M., Dikshit, R., Eser, S., Mathers, C., Rebelo, M., Parkin, D., Forman, D., Bray, F., 2013. GLOBOCAN 2012 v1.0, Cancer Incidence and Mortality Worldwide: IARC CancerBase No. 11 [Internet]. International Agency for Research on Cancer, Lyon, France. Available from: http://globocan.iarc.fr.
Flouriot, G., Huet, G., Demay, F., Pakdel, F., Boujrad, N., Michel, D., 2014. The actin/MKL1 signaling pathway influences cell growth and gene expression through large-scale chromatin reorganization and histone post-translational modifications. Biochem. J. 461, 257–268.

Gentleman, R., Carey, V., Bates, D., Bolstad, B., Dettling, M., Dudoit, S., Ellis, B., Gautier, L., Ge, Y., Gentry, J., Hornik, K., Hothorn, T., Huber, W., Iacus, S., Irizarry, R., Leisch, F., Li, C., Maechler, M., Rossini, A., Sawitzki, G., Smith, C., Smyth, G., Tierney, L., Yang, J., Zhang, J., 2004. Bioconductor: open software development for computational biology and bioinformatics. Genome Biol. 5, R80.

Guess, C.M., Quaranta, V., 2009. Defining the role of laminin-332 in carcinoma. Matrix Biol. 28, 445–455.

Gurbuz, I., Ferralli, J., Roloff, T., Chiquet-Ehrismann, R., Asparuhova, M., 2014. SAP domain-dependent Mkl1 signaling stimulates proliferation and cell migration by induction of a distinct gene set indicative of poor prognosis in breast cancer patients. Mol. Cancer 13, 22.

Hanna, M., Liu, H., Amir, J., Sun, Y., Morris, S.W., Siddiqui, M.A.Q., Lau, L.F., Chaqour, B., 2009. Mechanical regulation of the proangiogenic factor CCN1/CYR61 gene requires the combined activities of MRTF-A and CREB-binding protein histone acetyltransferase. J. Biol. Chem. 284, 23125–23136.

Heit, C., Jackson, B., McAndrews, M., Wright, M., Thompson, D., Silverman, G., Nebert, D., Vasiliou, V., 2013. Update of the human and mouse SERPIN gene superfamily. Hum Genomics 7, 22.

Hynes, R.O., Naba, A., 2012. Overview of the matrisome—an inventory of extracellular matrix constituents and functions. Cold Spring Harb. Perspect. Biol. 4, a004903.

Ivanov, S., Liao, S.Y., Ivanova, A., Danilkovitch-Miagkova, A., Tarasova, N., Weirich, G., Merrill, M.J., Proescholdt, M.A., Oldfield, E.H., Lee, J., Zavada, J., Waheed, A., Sly, W., Lerman, M.I., Stanbridge, E.J., 2001. Expression of hypoxia-inducible cell-surface transmembrane carbonic anhydrases in human cancer. Am. J. Pathol. 158, 905–919.

Jiang, P., Li, X., Thompson, C., Huang, Z., Araiza, F., Osgood, R., Wei, G., Feldmann, M., Frost, G., Shepard, H., 2012. Effective targeting of the tumor microenvironment for cancer therapy. Anticancer Res. 32, 1203–1212.

Kalluri, R., Zeisberg, M., 2006. Fibroblasts in cancer. Nat. Rev. Cancer 6, 392–401.

Kuonen, F., Laurent, J., Secondini, C., Lorusso, G., Stehle, J.C., Rausch, T., Faes-van't Hull, E., Bieler, G., Alghisi, G.C., Schwendener, R., Andrejevic-Blant, S., Mirimanoff, R.O., Rüegg, C., 2012. Inhibition of the Kit ligand/c-Kit axis attenuates metastasis in a mouse model mimicking local breast cancer relapse after radiotherapy. Clin. Cancer Res. 18, 4365–4374.

Le Scodan, R., Stevens, D., Brain, E., Floiras, J.L., Cohen-Solal, C., De La Lande, B., Tubiana-Hulin, M., Yacoub, S., Gutierrez, M., Ali, D., Gardner, M., Moisson, P., Villette, S., Lerebours, F., Munck, J.N., Labib, A., 2009. Breast cancer with synchronous metastases: survival impact of exclusive locoregional radiotherapy. J. Clin. Oncol. 27, 1375–1381.

Leitner, L., Shaposhnikov, D., Descot, A., Hoffmann, R., Posern, G., 2010. Epithelial Protein Lost in Neoplasm alpha (Eplin-alpha) is transcriptionally regulated by G-actin and MAL/MRTF coactivators. Mol. Cancer 9, 60.

Lemay, R., Archambault, M., Tremblay, L., Bujold, R., Lepage, M., Paquette, B., 2011. Irradiation of normal mouse tissue increases the invasiveness of mammary cancer cells. Int. J. Radiat. Biol. 87, 472–482.

Levental, K.R., Yu, H., Kass, L., Lakins, J.N., Egeblad, M., Erler, J.T., Fong, S.F.T., Csiszar, K., Giaccia, A., Weninger, W., Yamauchi, M., Gasser, D.L., Weaver, V.M., 2009. Matrix crosslinking forces tumor progression by enhancing integrin signaling. Cell 139, 891–906.

Li, T., Sun, L., Miller, N., Nicklee, T., Woo, J., Hulse-Smith, L., Tsao, M.S., Khokha, R., Martin, L., Boyd, N., 2005. The association of measured breast tissue characteristics with mammographic density and other risk factors for breast cancer. Cancer Epidemiol. Biomark. Prev. 14, 343–349.

Liu, X., Wu, H., Byrne, M., Krane, S., Jaenisch, R., 1997. Type III collagen is crucial for collagen I fibrillogenesis and for normal cardiovascular development. Proc. Natl. Acad. Sci. U. S. A. 94, 1852–1856.

Livak, K.J., Schmittgen, T.D., 2001. Analysis of relative gene expression data using real-time quantitative PCR and the 2(−Delta Delta C(T)) method. Methods 25, 402–408.

Lopez, J.I., Kang, I., You, W.K., McDonald, D.M., Weaver, V.M., 2011. In situ force mapping of mammary gland transformation. Integr. Biol. (Camb.) 3, 910–921.

Maier, S., Lutz, R., Gelman, L., Sarasa-Renedo, A., Schenk, S., Grashoff, C., Chiquet, M., 2008. Tenascin-C induction by cyclic strain requires integrin-linked kinase. Biochim. Biophys. Acta 1783, 1150–1162.

Mattsson, A., Rudén, B.I., Hall, P., Wilking, N., Rutqvist, L.E., 1993. Radiation-induced breast cancer: long-term follow-up of radiation therapy for benign breast disease. J. Natl. Cancer Inst. 85, 1679–1685.

Medjkane, S., Perez-Sanchez, C., Gaggioli, C., Sahai, E., Treisman, R., 2009. Myocardin-related transcription factors and SRF are required for cytoskeletal dynamics and experimental metastasis. Nat. Cell Biol. 11, 257–268.

Milas, L., Hirata, H., Hunter, N., Peters, L.J., 1988. Effect of radiation-induced injury of tumor bed stroma on metastatic spread of murine sarcomas and carcinomas. Cancer Res. 48, 2116–2120.

Minn, A.J., Gupta, G.P., Siegel, P.M., Bos, P.D., Shu, W., Giri, D.D., Viale, A., Olshen, A.B., Gerald, W.L., Massague, J., 2005. Genes that mediate breast cancer metastasis to lung. Nature 436, 518–524.

Miralles, F., Posern, G., Zaromytidou, A.I., Treisman, R., 2003. Actin dynamics control SRF activity by regulation of its coactivator MAL. Cell 113, 329–342.

Monnier, Y., Farmer, P., Bieler, G., Imaizumi, N., Sengstag, T., Alghisi, G.C., Stehle, J.C., Ciarloni, L., Andrejevic-Blant, S., Moeckli, R., Mirimanoff, R.O., Goodman, S.L., Delorenzi, M., Rüegg, C., 2008. CYR61 and αVβ5 integrin cooperate to promote invasion and metastasis of tumors growing in preirradiated stroma. Cancer Res. 68, 7323–7331.

Morita, T., Mayanagi, T., Sobue, K., 2007. Dual roles of myocardin-related transcription factors in epithelial mesenchymal transition via slug induction and actin remodeling. J. Cell Biol. 179, 1027–1042.

Muehlich, S., Wang, R., Lee, S.M., Lewis, T.C., Dai, C., Prywes, R., 2008. Serum-induced phosphorylation of the serum response factor coactivator MKL1 by the extracellular signal-regulated kinase 1/2 pathway inhibits its nuclear localization. Mol. Cell. Biol. 28, 6302–6313.

Nguyen, D.H., Oketch-Rabah, H.A., Illa-Bochaca, I., Geyer, F.C., Reis-Filho, J.S., Mao, J.H., Ravani, S.A., Zavadil, J., Borowsky, A.D., Jerry, D.J., Dunphy, K.A., Seo, J.H., Haslam, S., Medina, D., Barcellos-Hoff, M.H., 2011. Radiation acts on the microenvironment to affect breast carcinogenesis by distinct mechanisms that decrease breast cancer latency and affect tumor type. Cancer Cell 19, 640–651.

O'Brien, C., Smith, J., Soong, S., Urist, M., Maddox, W., 1986. Neck dissection with and without radiotherapy: prognostic factors, patterns of recurrence, and survival. Am. J. Surg. 152, 456–463.

O'Connell, J.T., Sugimoto, H., Cooke, V.G., MacDonald, B.A., Mehta, A.I., LeBleu, V.S., Dewar, R., Rocha, R.M., Brentani, R.R., Resnick, M.B., Neilson, E.G., Zeisberg, M., Kalluri, R., 2011. VEGF-A and tenascin-C produced by S100A4+ stromal cells are important for metastatic colonization. Proc. Natl. Acad. Sci. U. S. A. 108, 16002–16007.

O'Connor, J., Gomez, E., 2014. Biomechanics of TGFbeta-induced epithelial-mesenchymal transition: implications for fibrosis and cancer. Clin. Transl. Med. 3, 23.

O'Sullivan, B., Levin, W., 2003. Late radiation-related fibrosis: pathogenesis, manifestations, and current management. Semin. Radiat. Oncol. 13, 274–289.

Oskarsson, T., Acharyya, S., Zhang, X.H.F., Vanharanta, S., Tavazoie, S.F., Morris, P.G., Downey, R.J., Manova-Todorova, K., Brogi, E., Massague, J., 2011. Breast cancer cells produce tenascin C as a metastatic niche component to colonize the lungs. Nat. Med. 17, 867–874.

Paszek, M.J., Zahir, N., Johnson, K.R., Lakins, J.N., Rozenberg, G.I., Gefen, A., Reinhart-King, C.A., Margulies, S.S., Dembo, M., Boettiger, D., Hammer, D.A., Weaver, V.M., 2005. Tensional homeostasis and the malignant phenotype. Cancer Cell 8, 241–254.

Pickup, M.W., Laklai, H., Acerbi, I., Owens, P., Gorska, A.E., Chytil, A., Aakre, M., Weaver, V.M., Moses, H.L., 2013. Stromally derived lysyl oxidase promotes metastasis of transforming growth factor-β-deficient mouse mammary carcinomas. Cancer Res. 73, 5336–5346.

Provenzano, P.P., Cuevas, C., Chang, A.E., Goel, V.K., Von Hoff, D.D., Hingorani, S.R., 2012. Enzymatic targeting of the stroma ablates physical barriers to treatment of pancreatic ductal adenocarcinoma. Cancer Cell 21, 418–429.

Pulaski, B.A., Ostrand-Rosenberg, S., 2001. Mouse 4T1 breast tumor model. Curr. Protoc. Immunol. (John Wiley & Sons, Inc.). Chapter 20: Unit 20.2.

Ramirez, F., Sakai, L.Y., 2010. Biogenesis and function of fibrillin assemblies. Cell Tissue Res. 339, 71–82.

Ricard-Blum, S., 2011. The collagen family. Cold Spring Harb. Perspect. Biol. 3, a004978.

Ricciardelli, C., Sakko, A., Ween, M., Russell, D., Horsfall, D., 2009. The biological role and regulation of versican levels in cancer. Cancer Metastasis Rev. 28, 233–245.

Roy, D.M., Walsh, L.A., 2014. Candidate prognostic markers in breast cancer: focus on extracellular proteases and their inhibitors. Breast Cancer (Dove Med. Press) 6, 81–91.

Samani, A., Bishop, J., Luginbuhl, C., Plewes, D.B., 2003. Measuring the elastic modulus of ex vivo small tissue samples. Phys. Med. Biol. 48, 2183–2198.

Saupe, F., Schwenzer, A., Jia, Y., Gasser, I., Spenlé, C., Langlois, B., Kammerer, M., Lefebvre, O., Hlushchuk, R., Rupp, T., Marko, M., van der Heyden, M., Cremel, G., Arnold, C., Klein, A., Simon-Assmann, P., Djonov, V., Neuville-Méchine, A., Esposito, I., Slotta-Huspenina, J., Janssen, K.P., de Wever, O., Christofori, G., Hussenet, T., Orend, G., 2013. Tenascin-C downregulates Wnt inhibitor Dickkopf-1, promoting tumorigenesis in a neuroendocrine tumor model. Cell Rep. 5, 482–492.

Scharenberg, M.A., Pippenger, B.E., Sack, R., Zingg, D., Ferralli, J., Schenk, S., Martin, I., Chiquet-Ehrismann, R., 2014. TGF-β-induced differentiation into myofibroblasts involves specific regulation of two MKL1 isoforms. J. Cell Sci. 127, 1079–1091.

Schmittgen, T.D., Livak, K.J., 2008. Analyzing real-time PCR data by the comparative CT method. Nat. Protoc. 3, 1101–1108.

Schwartz, M.A., 2010. Integrins and extracellular matrix in mechanotransduction. Cold Spring Harb. Perspect. Biol. 2, a005066.

Smyth, G.K., Speed, T., 2003. Normalization of cDNA microarray data. Methods 31, 265–273.

Sun, M., Chen, S., Adams, S.M., Florer, J.B., Liu, H., Kao, W.W.Y., Wenstrup, R.J., Birk, D.E., 2011. Collagen V is a dominant regulator of collagen fibrillogenesis: dysfunctional regulation of structure and function in a corneal-stroma-specific Col5a1-null mouse model. J. Cell Sci. 124, 4096–4105.

Swift, J., Discher, D.E., 2014. The nuclear lamina is mechano-responsive to ECM elasticity in mature tissue. J. Cell Sci. 127, 3005–3015.

Swift, J., Ivanovska, I.L., Buxboim, A., Harada, T., Dingal, P.C., Pinter, J., Pajerowski, J.D., Spinler, K.R., Shin, J.W., Tewari, M., Rehfeldt, F., Speicher, D.W., Discher, D.E., 2013. Nuclear lamin-A scales with tissue stiffness and enhances matrix-directed differentiation. Science 341.

Tavazoie, S.F., Alarcon, C., Oskarsson, T., Padua, D., Wang, Q., Bos, P.D., Gerald, W.L., Massague, J., 2008. Endogenous human microRNAs that suppress breast cancer metastasis. Nature 451, 147–152.

Throm Quinlan, A., Sierad, L., Capulli, A., Firstenberg, L., Billiar, K., 2011. Combining dynamic stretch and tunable stiffness to probe cell mechanobiology in vitro. PLoS One 6, e23272.

Tsuruta, D., Kobayashi, H., Imanishi, H., Sugawara, K., Ishii, M., Jones, J.C.R., 2008. Laminin-332-integrin interaction: a target for cancer therapy? Curr. Med. Chem. 15, 1968–1975.

Vartiainen, M.K., Guettler, S., Larijani, B., Treisman, R., 2007. Nuclear actin regulates dynamic subcellular localization and activity of the SRF cofactor MAL. Science 316, 1749–1752.

Vicini, F.A., Kestin, L., Huang, R., Martinez, A., 2003. Does local recurrence affect the rate of distant metastases and survival in patients with early-stage breast carcinoma treated with breast-conserving therapy? Cancer 97, 910–919.

Vikram, B., Strong, E., Shah, J., Spiro, R., 1984. Failure at distant sites following multimodality treatment for advanced head and neck cancer. Head Neck Surg. 6, 730–733.

Walker, R., 2001. The complexities of breast cancer desmoplasia. Breast Cancer Res. 3, 143–145.

Wang, D.Z., Li, S., Hockemeyer, D., Sutherland, L., Wang, Z., Schratt, G., Richardson, J.A., Nordheim, A., Olson, E.N., 2002. Potentiation of serum response factor activity by a family of myocardin-related transcription factors. Proc. Natl. Acad. Sci. U. S. A. 99, 14855–14860.

Yang, Y., Chen, D., Yuan, Z., Fang, F., Cheng, X., Xia, J., Fang, M., Xu, Y., Gao, Y., 2013. Megakaryocytic leukemia 1 (MKL1) ties the epigenetic machinery to hypoxia-induced transactivation of endothelin-1. Nucleic Acids Res. 41, 6005–6017.

Yoshio, T., Morita, T., Tsujii, M., Hayashi, N., Sobue, K., 2010. MRTF-A/B suppress the oncogenic properties of v-ras- and v-src-mediated transformants. Carcinogenesis 31, 1185–1193.

Zhang, M., Fang, H., Zhou, J., Herring, B.P., 2007. A novel role of Brg1 in the regulation of SRF/MRTFA-dependent smooth muscle-specific gene expression. J. Biol. Chem. 282, 25708–25716.

Zhao, X.H., Laschinger, C., Arora, P., Szaszi, K., Kapus, A., McCulloch, C.A., 2007. Force activates smooth muscle alpha-actin promoter activity through the Rho signaling pathway. J. Cell Sci. 120, 1801–1809.